MAGIC-TDAS 04-04
041207/AMoralejo

Monte Carlo estimate of flux sensitivity of MAGIC for point-like sources

A. Moralejo
<moralejo@pd.infn.it>

December 7, 2004

Abstract

An update of the Monte Carlo estimate of the MAGIC flux sensitivity for point sources is presented. A number of improvements in the MC camera simulation have been made in the last few months, rendering the simulation more realistic. Predictions of observed fluxes for the Crab nebula in different energy ranges have been included.

Contents

1 Introduction

A new version (0.7) of the MAGIC camera Monte Carlo simulation was released recently [9]. Since then we have been working in the tuning of the camera simulation parameters, in order to reproduce the behaviour of the real telescope as precisely as possible. Some results on the comparison of MC and data have been presented in past meetings, and a note with more detailed explanations will follow soon. Although the agreement is not yet fully satisfactory (and perhaps it will never be, given the necessary idealizations in the simulation), we consider it good enough as to attempt a rough estimate of the flux sensitivity of MAGIC. Sensitivity is a key parameter for instance in the process of selecting target sources and allocating observation times, and hence it is rather convenient to have an updated estimate for the preparation of the coming Physics campaigns.

A draft of the present note was made public in July 2004. This is a much updated version in which some details of the simulation and the analysis have been changed, as well as the studied telescope setups. The results are basically the same as presented in the draft, but different aspects of the study have been checked, and many details on the analysis have been added to this version. Although this has made the note a bit too bulky, we think it is fundamental to guarantee the reproducibility in the future of the results here presented, and to facilitate the finding of possible errors. We want to avoid the repetition of the situation created by the claims in the Monte Carlo chapter of the MAGIC design report (now known at least in part to be wrong). These have been for long time (and still are) a riddle for those of us trying to confirm them, due to the absence of a detailed description of the work.

2 The Monte Carlo sample

Regarding the shower generation, atmospheric absorption and reflection on the mirror, the MC library used here is in all respects similar to that used in previous studies of the same kind [8]. Only the statistics have changed. We are now using 2.6×10^7 protons between 30 GeV and 30 TeV (spectral index -2.75), 1.3×10^7 helium nuclei in the same range (-2.62), and 7.8×10^6 gammas between 10 GeV and 30 TeV (-2.6) [1]. A slightly modified version of CORSIKA 6.019 [12] (with VENUS for hadronic interactions) was used for the shower generation. This program, adapted from CORSIKA by D. Sobczyńska, is what we call MMCS [22]. The maximum impact parameter is 400 m for hadrons and 300 m for gammas. Directions of hadrons were scattered isotropically in a 5 degree semiaperture cone around the telescope direction. Gammas have all the same incident direction, paralel to the telescope axis (simulating a point-like source). The telescope pointing directions range from 0 to $\simeq 30^\circ$ in zenith angle θ (flatly distributed in $\cos\theta$), and ϕ angles are 0 and 90° (half the events at each azimuth angle). For the definition of the azimuth used here, see [21].

We have incorporated also a high energy proton sample, containing 5.2×10^6 events above 200 GeV. The latter will permit to extend the sensitivity estimation beyond the energies considered in previous studies. All the used MC *reflector* files, which correspond to zenith angle bins 0 to 12, are available at the Padua web pages [1], under the directories labeled *STD* (standard) and *HE* (high energy).

2.1 Absolute normalization of hadron flux

Another difference with previous studies is that the absolute flux normalization at 30 GeV for protons and Helium nuclei have now been taken from AMS-01 measurements [4, 5], from which we derived the

[1] The spectrum of the gamma events used in the **training** of the γ/hadron separation method has been modified as discussed in section §4.

following differential spectra:

$$\frac{dN_p}{dE\ dS\ dt\ d\Omega} = 1.338 \times \left(\frac{E}{30\ \mathrm{GeV}}\right)^{-2.78}\ \mathrm{GeV}^{-1}\ \mathrm{m}^{-2}\ \mathrm{s}^{-1}\ \mathrm{sr}^{-1} \tag{1}$$

$$\frac{dN_{He}}{dE\ dS\ dt\ d\Omega} = 0.755 \times \left(\frac{E}{30\ \mathrm{GeV}}\right)^{-2.74}\ \mathrm{GeV}^{-1}\ \mathrm{m}^{-2}\ \mathrm{s}^{-1}\ \mathrm{sr}^{-1} \tag{2}$$

Using these expressions, the integrated rates of protons and Helium nuclei above 30 GeV, in a 400 m radius circle and 5 degree semiaperture cone, turn out to be 2.7566×10^5 and 1.6803×10^5 Hz respectively.

Formerly we had been using older measurements taken from [24]. From these, we produced our MC sample using power law differential spectra -2.75 and -2.62, for protons and He respectively. The former index is compatible within the uncertainties with the AMS measurement, while the latter is significantly smaller. We have not corrected for this difference in the present work, and so the Helium contribution will be slightly overestimated (the difference in the integrals between 30 GeV and 30 TeV due to the change in the spectral index is only of about 7%). In all, these new measurements result in absolute fluxes which are $\simeq$ 20% lower for protons, and a $\simeq$ 17% higher for Helium nuclei, hence resulting in lower total background rates than those assumed previously [8].

Another factor which makes background rates lower than those reported for instance in [8] is the use of a more realistic telescope optics in this work (see §3).

2.2 The rates in the MAGIC TDR

As for the proton rates in the MAGIC technical design report (TDR) [7], they are wrong, too low because of an error in the generation of random directions of the simulated proton showers. A prediction of a $\simeq$ 13 Hz rate of protons is made there (p. 170), for a setup with a gamma peak energy around 30 GeV. As comparison, the lowest energy sample we will present here, which has a peak energy $E_0 = 36.5$ GeV before cuts (see table 3), has a proton rate of 196 Hz. Taking into account that the trigger area in the TDR was smaller by a factor 1.44 than the current one, we end up with a subestimation of proton rate of around a factor 10 (we would have to add also the rate of He nuclei, which is not negligible). This is one of the reasons (but possibly not the only one) for the very high sensitivity predicted in the design report. I remind this here, because people starting to work in MAGIC often gets confused about the discrepancies between our current numbers (both from the MC and the data) and those in the TDR. A recent e-mail discussion suggests also that some MAGIC collaborators still believe that the sensitivity predicted in the TDR would hold for a high QE camera like the one described there. Unfortunately, we know that this will not be the case (see §7.4).

2.3 Electron rates

Electrons have not been considered in this study. Electrons would consitute an irreducible background since they produce purely electromagnetic showers, like gammas. The only possible discrimination is the one related to the shower orientation if the gamma ray source is a point-like one. In any case, estimates made by C. Bigongiari (see [20], p. 25) indicate that the electron contribution to the remaining background after analysis will be rather negligible: at low energies the residual hadronic background dominates, since the hadron supression is quite poor (see §7.1), and the incoming electron flux is intrinsecally much lower than that of protons [3, 5]. As one goes up in energy, the *residual* hadronic rate drops dramatically as the hadron identification becomes more and more efficient, but so does the electron rate, because the cosmic electron spectrum is steeper than that of nuclei.

3 Camera simulation

Details of the camera simulation version 0.7 can be found in [9]. Here we will simply list the most relevant improvements and changes with respect to the camera simulation (v. 0.6) used in [8]:

- The low gain branch is now simulated. In the MC, the gain ratio to the high gain branch is a factor 10 (same for all pixels).

- The shape of the single photoelectron response is no longer a gaussian of FWHM 5 ns, but has been obtained from measurements performed by F. Goebel with the *Pulpo* setup. Also the pulse is now more centered in the FADC window than it used to be, closer to what is observed in the real data. However, the shape of the simulated pulse in the low gain branch is the same as the one in the high gain. We know this is not the case in real data, where low gain pulses are wider, but this is yet to be implemented in the MC.

- It is now possible to blur the shower images during the camera simulation. Each one of the coordinates (x,y) of the photons on the camera plane is randomly smeared following a gaussian whose sigma in cm can be specified in the camera simulation input card. This smearing is additional to the "intrinsic" PSF which has been set into the reflector simulation (where the default spot has a projected RMS in each axis of $\simeq 0.7$ cm: a combination of the intrinsic spot size of each mirror element and small random misalignments of the elements [21]).

  In this work we have used an additional smearing of $\sigma = 1$ cm. Given that the telescope is focused at 10 km distance, this means that the spot produced by a point-like source placed 10 km away along the telescope axis would have $\sigma = \sqrt{0.7^2 + 1^2} = 1.22$ cm, that is, $0.41°$. This has been estimated as the most likely value by K. Mase, following the study of muon rings [15] in real data taken after the August intervention, during which the mirror dish was completed and the panels set in chessboard pattern. Note that the chessboard structure has not been simulated for the present studies, but since timing has not been used in the analysis, this should not make any difference. All the spot sizes quoted above are the sole result of the quality of the mirrors and the goodness of their alignment. Coma aberration, which is *naturally* incorporated by the ray tracing routines, would produce an *additional* enlargement of the spot for light arriving off the telescope axis. In figures 11 and 13 of TDAS 02-11 [21], the effect of aberration can be seen.

- It is possible as well to simulate an incomplete mirror surface when running the camera simulation (the necessary fraction of photons is simply eliminated by the program). The same input card command (*mirror_fraction*) can be used to simulate any other loss of light collection efficiency, even if not due to the mirror (for instance lower QE). In the current work we have assumed a light collection efficiency, with respect to the one simulated by default, of 73% (see table 1). We have chosen this factor because it seems to match well with the results of the muon analysis by K. Mase [15]. Muons are for the moment the only way we have to estimate our true light collection capacity (including the mirror and the photon to photoelectron conversion). We realized also that the agreement between real cosmic ray events and MC hadrons (protons + helium nuclei) in all tested shower parameters became better by assuming this light loss of 27%. Direct measurements of the mirror affective surface and reflectivity, and of QE, will be available in the future.

- Average conversion factor from photons to photoelectrons, including the effect of the plexiglas window, light guides and first dynode phe$^-$ collection efficiency, has now been tuned to the value estimated by D. Paneque for the real inner pixels (after the coating). The average value (for Cherenkov photons) has then moved from $\simeq$ 23% to $\simeq$ 18%. The light collection efficiency of outer pixels, formerly assumed equal to that of inner ones, is now a factor 1/3 lower ($\simeq$ 12%), a number drawn from the calibration of real data with the F-factor method [11].

- The electronic noise (switched off in the simulation used in previous studies) has been added, the used value has been obtained from the analysis of a pedestal run taken with closed camera on September 21, 2004. One has to remember that, since in the simulation the electronic noise in the different FADC slices is generated independently (whereas in the data there are correlations), the tuning of the noise parameters in the MC camera simulation will depend slightly on the signal extraction method employed in the analysis.

- The contribution of diffuse NSB, based on the total flux from a dark patch of sky as reported in [18], has been recalculated to be, for the coated PMTs, around 0.13 phe$^-$ / ns / inner pixel (0.09 in former studies). The comparison of the noise fluctuations in a real data (open lid) pedestal file with those seen in the MC when an "empty" (i. e., without showers) reflector file is processed, shows rather good agreement (see fig. 1). Actually the fluctuations in outer pixels for the MC are slightly larger, but the difference is much smaller than the variations seen on real data from run to run, and on different sky regions.

- The gain of the electronics chain has been adapted to the values obtained from the calibration of real data (in particular from 21/09/2004), to have roughly the same average conversion of ADC counts to photoelectrons. We have also set a lower gain in outer pixels than in inner ones, as in the real data, so that the response of the whole camera is "flat" for a given light density (signal proportional to light density, and not to absolute number of photons within a pixel). In the simulation, however, the conversion factor of all inner pixels is the same, as well as that of all outer pixels, whereas in real data they vary from pixel to pixel.

- A time jitter of $\pm$ 0.5 slices in the position of the pulses in the FADC has been introduced. This simulates the FADC clock noise, and is a "coherent" jitter for all the pixels in an event. This is the only feature of the camera simulation used in this work which is not available in the released camera 0.7. A new release of camera will be made early in 2005 containing this and other new features.

In table 1 the main parameters used in the MC simulation for this work are summarized.

4 The analysis method

4.1 Signal extraction

The results presented here have been obtained in much the same way as those in [8] and [20]. We have used a different Mars signal extraction method, called *MExtractFixedWindowPeakSearch* which looks for the position in the FADC window of the highest non saturated high gain signal for every event, and around it defines a fixed integration window for all pixels in that event. This method is now convenient for MC events also, since we have introduced the jitter in the pulse positions (see above). The highest signal among pixels is searched adding 4 consecutive slices, and looking in the whole range of the high gain FADC slices. The width we have chosen for the integration window, both

Mirror Size		$956 \times 0.495^2 = 234.24$ m^2
$\langle$ Mirror reflectivity $\rangle$		0.85 (λ dependence as in [21])
Telescope focusing distance		10 km (camera plane at f + 3 cm)
Mirror PSF, projected 1-d σ		0.041° (spot from point source on-axis 10 km away)
Photon conversion efficiency and gain		
$\left\langle \frac{\text{Photoelectrons in } 1^{st} \text{ dynode}}{\text{Photons before plexiglas}} \right\rangle$	Inner pixels	0.183 phe$^-$/photon
	Outer pixels	0.122 phe$^-$/photon
QE vs λ, shape		As in fig. 5 of [9]
$\left\langle \frac{\text{Pulse integral FADC counts}}{\text{Photoelectrons in } 1^{st} \text{ dynode}} \right\rangle$	Inner pixels	7.8 FADC counts / phe$^-$
	Outer pixels	3.2 FADC counts / phe$^-$
Single phe$^-$ response shape		"Pulpo", as in fig. 1 of [9]
PMT gain fluctuations		As in fig. 6 of [9]
Correction factor to light collection efficiency		0.73 (see caption and text)
Noise		
$\langle$ Diffuse NSB noise $\rangle$	Inner pixels	0.130 phe$^-$/ns
	Outer pixels	0.347 phe$^-$/ns
NSB from individual stars		Not simulated
Electronic noise per slice, σ of gaussian (scales down in LG branch)	Inner pixels	1.3 FADC counts
	Outer pixels	2.4 FADC counts
Additional electronic noise per slice in FADC, σ of gaussian (same for HG and LG)		1 FADC count
Trigger		
Single phe$^-$ response at discr. input		gaussian, 2 ns FWHM, 1 mV amplitude
Discriminator threshold		4 mV
Discriminator output		squared, 3 ns duration
Trigger multiplicity and topology		4 close-compact next neighbours above threshold minimum overlap 0.25 ns

Table 1: *Main parameters of the Monte Carlo Reflector and Camera simulation used in the present study. The last row before the Noise section displays the correction factor to the overall light collection efficiency. This is a parameter that is set in the camera input card through the command "mirror_fraction", and it accounts not only for possibly missing, faulty or unfocused mirrors, but also for lower transmission of the camera plexiglas, or lower PMT QE than assumed by default in the simulation. The diffuse NSB values shown are the effective ones, after accounting for the correction factor (in the camera input card one has to set a value of 0.178 phe$^-$/ns/inner pixel to obtain $0.73 \times 0.178 = 0.130$; the scaling of the NSB for outer pixels is made automatically by the program).*

for high and low gain, is 6 FADC slices (20 ns). This is achieved by calling *MExtractFixedWindow-PeakSearch::SetWindows(6,6,4)*. In the first draft of this note a 8-slice window was used. We have changed this value to 6, which has been more frequently used in the analysis of our real data, but the results have not changed significantly. In even older studies, like those in [8], we had simulated lower noise, higher photon conversion efficiency, and integrated only 3 FADC slices. We therefore expect some increase of the energy threshold with respect to that work.

4.2 Check of the noise contribution

On figure 1 we show the comparison of the noise assumed in this MC simulation and that from a dark patch of sky. In the plots one can see the distribution of extracted signal (sum of 6 slices, in photons) for real and MC pedestal files, both for inner and outer pixels. The agreement is not perfect, but in real data variations from run to run and on different sky regions are bigger than the observed differences, so we deem that the simulated noise level is satisfactory. The FWHM of the curves for inner and outer pixels are respectively 27 photons and 78 photons. This would correspond to $\sigma = 11.5$ and 33.2 photons, or 2.1 and 4.05 photoelectrons. If we compute the contribution of the electronic noise alone, we get $\sigma = 0.558$ and 2.16 photoelectrons (all values are summarized in table 2). We see that the relative importance of electronic noise is much higher in outer pixels. This is the case also in the real data. So the noise in outer pixels (in terms of photons or phe$^-$) can be reduced by increasing their gains, although this will imply that they will saturate at a lower signal level. This issue probably deserves a deeper study.

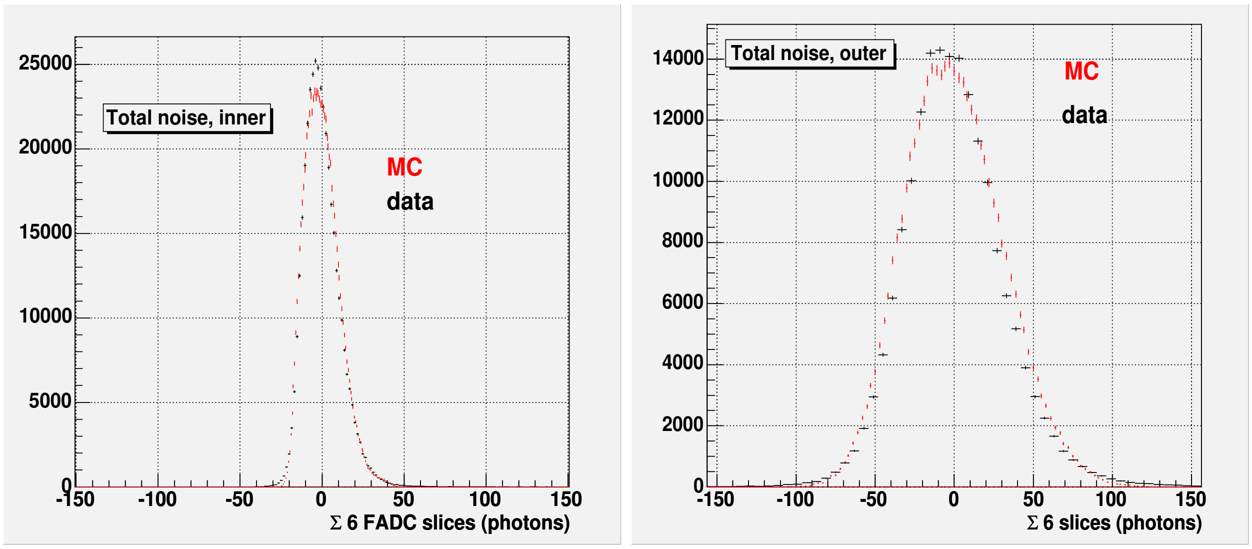

Figure 1: *Distribution of pixel signals (sum of 6 FADC slices) for a real pedestal run taken with open camera (21/9/2004, pointing to OffCrab-11, a dark patch of sky), and for a MC file with electronic noise and diffuse night sky background (but no showers). The total noise fluctuations observed in the data seems to be reasonably well reproduced in the MC. The NSB dominates clearly over electronic noise for inner pixels, whereas the two noise contributions are comparable for outer pixels due to the lower gain.*

4.3 Tail cuts

A classical image cleaning is performed on the images, with tail cuts set at 3 and 2 σ, and just one "ring" around *core* pixels being considered for the second tail cut[2]. These tail cuts are in units of the RMS (referred to as "σ" in the following) of the noise as calculated by Mars, which result of multiplying the square root of the number of integrated slices times the RMS of the noise in the single slice, as stored in *MMcFadcHeader.fPedesSigmaHigh*. The latter value is calculated by the camera simulation by performing a kind of pedestal run of 500 events, before running over showers. In reality the stored values are not the RMS of the noise in a single slice, but the RMS of the sum of 14 slices divided by $\sqrt{14}$. When we later multiply this by the square root of the number of summed slices, we get something which is close to the true RMS of the noise[3]. Due to correlations in the noise of neighbouring slices (think for instance in single phe$^-$ from NSB), it would not be convenient to store the true RMS of a single slice in order to estimate the fluctuations of the integrated noise.

Although the simulated noise is the same in all pixels, the calculation described above, based on just 500 events, yields slightly different values for different pixels. In average this "σ" of noise is 10.8 photons for inner pixels (the RMS of the distribution for all inner pixels is $\simeq 0.3$ photons). The tail cuts are then 32.5 and 21.6 photons, or 5.94 and 3.96 photoelectrons for inner pixels (table 2).

In the present default cleaning procedure of Mars, used here, the tail cuts for outer pixels are scaled up by a factor $\sqrt{4} = 2$. So they would be 6 and 4 times the RMS of the noise in outer pixels, which is in average 31.9 photons as calculated by Mars. Then this means tail cuts of 192 and 128 photons, or 23.4 and 15.6 photoelectrons. The scaling of the outer pixels tail cuts in Mars is intended to make that, in terms of photons per unit area, they are the same as for inner pixels. But this works only under two assumptions: that all or most of the noise is due to NSB (and hence fluctuations scale with the square root of the pixel area), and that the light collection efficiency of inner and outer pixels is the same (whereas at present time the outer pixels seem to be around a 30% less efficient). Expressed in terms of photons *per area of an inner pixel*, the outer tail cuts are 48.0 and 31.8 photons, and therefore they are about 46% higher than those for inner pixels. It would be better to change the *default* cleaning such that the tail cuts in terms of light density were the same for all of the camera.

4.4 Image parameters

After the cleaning, the moments of the light distribution on the camera are calculated. We use a set of basic parameters: ALPHA, DIST, SIZE, scaled WIDTH, scaled LENGTH, CONC, and third moment along major axis (with a sign containing the head-tail information with respect to the nominal source position - the center of the camera). In *Mars* this would be $MHillasExt.fM3Long \times sign(MHillasSrc.fCosDeltaAlpha)$. CONC is the ratio of the sum of the signals in the two highest pixels over SIZE. We tried using also CONC7 (sum of highest 7 pixels over SIZE), as suggested in the MAGIC design report [7], but we did not get any improvement in discrimination, and so it was discarded. Actually, for the smallest showers, with seven or fewer pixels, CONC7 equals one and is obviously useless for separation. For scaling WIDTH and LENGTH we have used a simple straight line fit to the profile histograms of WIDTH vs. $\log_{10}$ SIZE and LENGTH vs. $\log_{10}$ SIZE. The scaled

[2]In the first draft of this note, tail cuts were set at 4 and 3 σ. Again, the only visible effect of the change was a slight difference in energy threshold, but not on sensitivity.

[3]This method is just a patch which can be avoided if at the time of calculating the RMS of the noise one knows already the signal extractor to be used. In table 2 one can see that in this case the noise is correctly estimated, within 5%, by this procedure

parameters would then be

$$\text{SWIDTH} = \frac{\text{WIDTH}}{\langle\text{WIDTH}\rangle_{\log_{10}\text{SIZE}}} \qquad \text{SLENGTH} = \frac{\text{LENGTH}}{\langle\text{LENGTH}\rangle_{\log_{10}\text{SIZE}}} \tag{3}$$

Where the average values of WIDTH and LENGTH for each $\log_{10}$SIZE bin are taken from the linear fits (the expressions can be found in table 2). Actually the results do not improve much by using SWIDTH and SLENGTH instead of their unscaled counterparts. This indicates that Random Forest (see below) seems to take care of the SIZE dependence quite well by itself. In this sense, we will not gain anything significant by using more complex parametrizations of these shape parameters as a function of SIZE.

It must be noted that the used set of parameters is a rather simple one: it includes the most popular discriminators used by the previous generation Cherenkov telescopes, and hence we do not claim them to be optimal for low energies.

4.5 Absolute calibration and SIZE cuts

The Monte Carlo data have been calibrated during the calculation of image parameters (using the Mars macro starmc.C). For the calibration we correlate the SIZE values for gamma-initiated showers (from a MC file without noise) with the total number of Cherenkov photons arriving on the camera (which is known in the simulation). The output of starmc.C is a file containing image parameters with the SIZE values in number of photons. The conversion factor obtained for inner pixels is 0.139 phe$^-$ / FADC count. Note that this is not exactly the inverse of the camera simulation input gain (7.8 FADC counts / phe$^-$, see table 1), since when extracting the signal we are integrating 6 slices, and part of the pulse is beyond them (this effect is enhanced by the fact that we use the same integration window for all pixels in an event). For outer pixels the conversion factor is 0.339 phe$^-$ / FADC count.

Applying different cuts in Size ($>$ 0, 300, 500, 750, 1000, 1500, 1999, 2000, 3000, 4000, 5000, 6000 and 7000 photons) we can study the telescope performance at different energies. For the cuts at 2000 photons or above, we have used as sole background the high energy proton sample, above 200 GeV (and no Helium nuclei, neither low energy protons). We have applied correction factors to the total background rate to correct for these missing background events. The sample with SIZE $>$ 1999 photons has been used to check that the results obtained with the low energy hadron sample (p+He) and the high energy one (only p) are consistent. All the analysis described in the following has been performed for each one of these samples independently. A summary of all relevant quantities involved in the analysis is presented in tables 2, 3 and 4.

4.6 Hadronic background discrimination

For the classification of the events in hadron- or gamma-like, we have used the Random Forest method [13, 10], with the above mentioned image parameters except ALPHA. The number of trees is 100, the node size is 10 events and the number of trials in random split selection is 3 (see [13] for the meaning of these parameters).

The MC library was divided into two independent sets of events, a training sample and a test sample. The gamma training sample was modified (by eliminating events) such that the SIZE distribution would match that of the hadron sample (protons + Helium nucleii). The intrinsic SIZE distributions of gammas and hadrons are different, both because of the different energy spectra and because of the effect of the trigger on the different shapes of gamma and hadron images. However, we do not want SIZE to be used as a separation parameter in itself, but just as a scaling parameter, since the

Signal extraction	*MExtractFixedWindowPeakSearch::SetWindows(6, 6, 4)*		
Absolute calibration	Inner pixels	0.139	phe$^-$/ FADC count
	Outer pixels	0.339	phe$^-$/ FADC count
Electronic noise, σ	Inner pixels	0.558	phe$^-$ = 3.05 photons
	Outer pixels	2.16	phe$^-$ = 17.7 photons
Total noise, σ	Inner pixels	2.10	phe$^-$ = 11.5 photons
	Outer pixels	4.05	phe$^-$ = 33.2 photons
IMAGE CLEANING			
Cleaning method	*MImgCleanStd::kStandard, (3σ, 2σ), 1 ring*		
σ of noise, Mars estimate	Inner pixels	1.98	phe$^-$ = 10.8 photons
	Outer pixels	3.89	phe$^-$ = 31.9 photons
Tail cut 1 (3 σ)	Inner pixels	5.94	phe$^-$ = 32.5 photons
	Outer pixels	23.3	phe$^-$ = 191 photons
Tail cut 2 (2 σ)	Inner pixels	3.96	phe$^-$ = 21.6 photons
	Outer pixels	15.6	phe$^-$ = 128 photons

IMAGE PARAMETERS USED FOR BG DISCRIMINATION

SIZE, DIST, CONC, M3LONG*
WIDTH[°] / $(-0.028235 + 0.03231 \times \log_{10}$ SIZE[phot])
LENGTH[°] / $(-0.13527 + 0.09876 \times \log_{10}$ SIZE[phot])
ALPHA (simple cut, not included in Random Forest)

Table 2: *Details on the analysis applied in this work. The total noise is not gaussian; the σ values reported as "Total noise" are simply the FWHM of the curves in fig. 1, divided by 2.35. The parameter CONC is calculated as the ratio of the sum of signal in the two highest pixels divided by SIZE. * M3LONG, the third moment of the image along the major axis, is calculated with a sign which is positive if the image is pointing as a gamma shower would (head closer to the source position than tail).*

shape parameters (WIDTH, LENGTH, longitudinal 3^{rd} moment...) depend on it. In his application of Random Forest to real data analysis, K. Mase [16] realized that at very low SIZE values, where the images are not much larger than a few pixels, the effectiveness of shape parameters as discriminators becomes quite poor, and the Random Forest starts making use of SIZE as a pure separation parameter, tagging events as gamma-like or hadron-like just because of their SIZE value. Of course this does not make much sense, since we do not know a priori the energy spectrum of the observed gamma sources, on which the SIZE distribution depends. This is the reason why we have modified the gamma training sample. On top of the modification of the SIZE spectrum, the gamma train sample has also been reduced to a number of events at most 50% larger than that of hadrons. This has been made to speed up the training: in the MC we have a much larger sample of triggered gammas than hadrons, and the performance of Random Forest does not improve by increasing the training statistics of just one of the two populations that one wants to discriminate.

The gamma **test** samples have not been modified, and consist of all the events fulfilling the corresponding SIZE cut, since we want to calculate the sensitivity for a source with differential spectrum dN/dE $\propto$ E$^{-2.6}$, which is precisely how the MC gammas have been produced.

4.7 Choosing the hadronnes cut

The chosen hadronness cut after running the MC test sample through the random forest, was usually the one which maximized the quality factor $Q = \varepsilon_\gamma/\sqrt{\varepsilon_h}$, being ε_γ and ε_h the surviving fractions of gammas and hadrons. These efficiencies ε_γ, ε_h, are referred **exclusively** to the effect of the γ / hadron separation, that is, they do not include the efficiency of the SIZE cut (which is not a γ / hadron separation cut).

The graphical output of Random Forest for a few of the samples is shown in figures 3 to 6. Be aware that direct comparison of these plots with the equivalent ones from [8] or some other works is not possible, because in this case ALPHA is not included in the γ/hadron discrimination. Whenever no clear local maximum of Q was seen (often the Q-factor curve is always rising for increasingly tight hadronness cuts, as in the bottom left graph of fig. 3), we chose somewhat arbitrarily a cut which kept 50% of gammas (leaving some room for the subsequent ALPHA cut, so that in all cases, not much less than half of gammas from the original sample will be kept after the full analysis). In all cases we have avoided choosing cuts in the region where Q fluctuates strongly due to the small number of hadron events after cuts: for instance, in the case SIZE > 4000 photons (fig. 6) we conservatively took a cut keeping 80% of gammas.

With respect to previous works we have excluded from the parameters used in background reduction the telescope zenith angle θ, which was hardly of any help, given that all the used MC events are contained in a relatively small range ($\theta < 30°$).

4.8 The ALPHA cut

In [8], ALPHA was also included among the parameters fed to the Random Forest. As shown in [20], including ALPHA together with the other parameters in the growing of the Random Forest does not increase significantly the separation power of the method, with respect to simply making a sharp cut in ALPHA after the γ/hadron separation has been made based on the other parameters. This is the approach we will use now. An additional advantage is that the statistics of triggered hadron events is quite limited (and much more so after SIZE cuts), and if ALPHA is included, the number of hadron events after separation is so low that very often it is difficult to estimate what is the optimal cut and what fraction of hadrons survives it. By excluding ALPHA, the statistics of hadrons after cuts increases, and then we can estimate how many would be further rejected by the ALPHA cut, by making an assumption on the shape of their ALPHA distribution.

4.9 Residual background rate estimate

For each of the samples with different SIZE cuts, the alpha distribution of hadrons **before** γ/hadron separation was fitted to a straight line to estimate the background in the low alpha region. For the gammas, for which we have much higher statistics, we took the ALPHA distribution **after** γ/hadron separation (and no fit was necessary). The ALPHA cut was decided, once more, as the one which made maximum the ratio of the number of surviving gammas over the square root of the number of surviving hadrons. For estimating the number of hadrons within a certain ALPHA range, we used the fitted straight line. To obtain the final number of hadrons, we applied the hadron efficiency factor from the optimal γ/hadron separation cut as defined in the previous section. In all this we are making an assumption, namely that the ALPHA distribution of hadrons is independent of the applied hadronness cut. It is known that at least some cuts on the shape parameters may lead to alterations of the ALPHA distribution of hadrons. The small statistics of our MC hadron library after separation does not allow us to prove beyond any doubt that this is not the case for our analysis, but at least a visual comparison of the fitted lines with the (few) surviving hadrons (see right pads of figures 8 to 11) seem to point to a rather good agreement.

We have not applied ALPHA cuts of less than 5°. Sometimes the optimal cut was just above 3°, but the improvement with respect to 5° was never large, and we have chosen not to apply such a sharp cut, which would require a perfect pointing over the full data taking period.

5 Definition of flux sensitivity

5.1 Minimum observable flux

The definition and calculation of flux sensitivity as reported in this study are the same as in [8]. It is the rather standard definition of "5 σ in 50 hours", assuming a point-like source with differential energy spectrum $dN/dE \propto E^{-2.6}$. The expression for the minimum observable integral flux is:

$$\phi^{min}_{E>E_0} = \frac{5}{A} \cdot \sqrt{\frac{R_h}{t_{50}}} \cdot \left(\frac{E_0}{10\ \mathrm{GeV}}\right)^{-1.6} \cdot \frac{N_{\gamma,\,prod}}{N_{\gamma,\,final}} \tag{4}$$

In this formula $A = \pi \times (300\ \mathrm{m})^2$ is the area (on the plane orthogonal to the observation direction) in which the MC gamma events have been produced, R_h is the residual hadron rate after all cuts, t_{50} is 50 hours, E_0 is the energy at which the differential energy spectrum of gammas peaks **after all cuts**, 10 GeV is the lower end of the energy range for the production of MC gammas, $N_{\gamma,\,prod}$ is the number of produced gamma showers (before trigger) and $N_{\gamma,\,final}$ is the number of gammas surviving all cuts. The last two numbers are obviously those of the **test** sample only. The formula is explained in more detail in [8]. Since in the analysis cuts we include the ALPHA cut and the simulated source is a point-like one, the flux sensitivities quoted in this work are only valid for point sources. All the numbers which are used in the formula can be found in table 3 and 4 ($N_{\gamma,\,final}$ is simply $N_{\gamma,test}$ after the ALPHA cut).

In the first draft of this study, and in older ones, we calculated E_0 as the peak energy of gammas before cuts. It is more reasonable to do it after all cuts, since we want to know the characteristic energy of the events that we succesfully identify as gammas. After cuts the energy peak usually shifts to slightly higher values, but the effect on sensitivity is very small because in our definition the minimum observable flux scales with $E_0^{-1.6}$ (see eq. 4).

Also keep in mind that the "5 σ" does not refer directly to the statistical significance of the signal one would obtain in 50 hours. It simply refers to the flux which would result, after all cuts, in a number of gammas equal to 5 times the standard deviation of the background fluctuations. This would translate in a statistical significance of 5 σ only in the ideal case in which the average expected background was perfectly known, which of course never happens in reality. For the case of a traditional "ON - OFF" analysis with equal time allocations for ON and OFF, the true significance in 50 hours would be in average a factor $\sqrt{2}$ smaller. It would then take 100 hours of ON-time to obtain a true 5 σ excess for the "minimum observable flux", plus the corresponding 100 hours of OFF source observations. This can be probably improved with wobble mode observations [25] which would eliminate the need for OFF data taking, and which would allow to get a better background estimate (from multiple OFF regions on the camera, away from the source position). Wobble mode would also imply a loss of collection

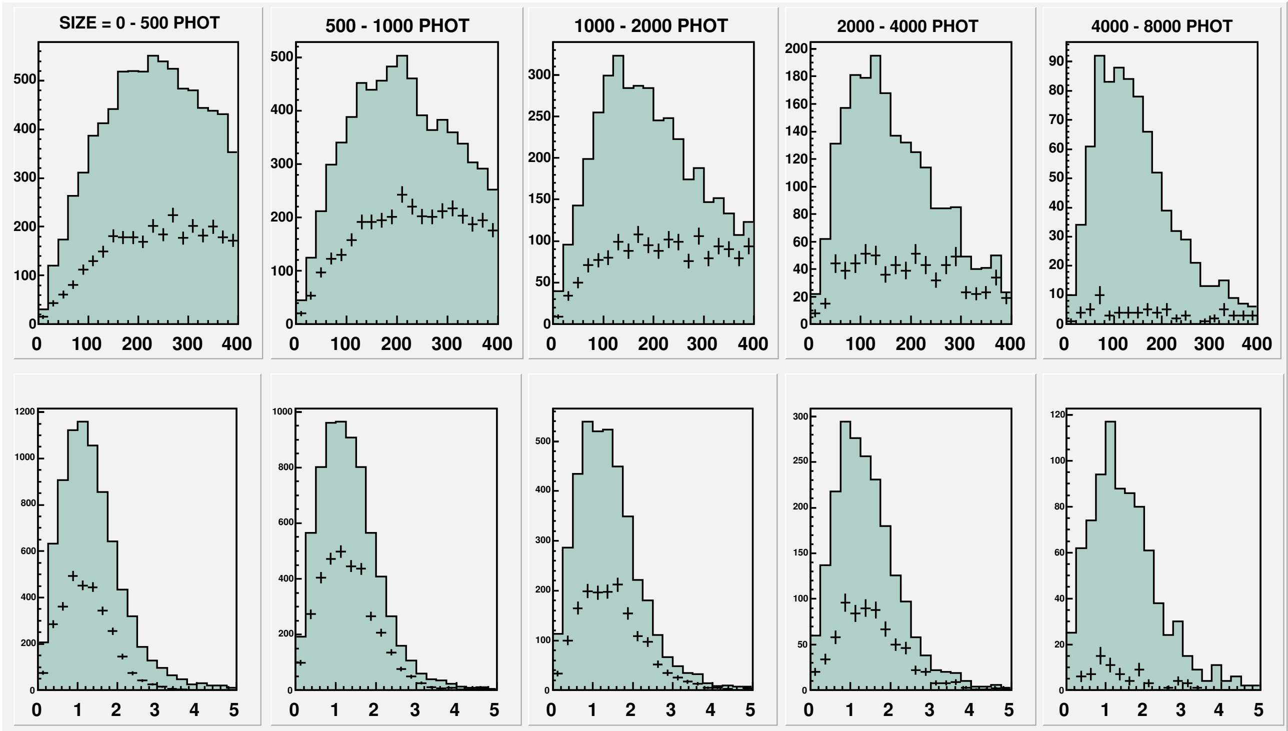

Figure 2: *Study of the so called "convergence" of the MC hadron library. The top row of plots shows the distribution of impact parameters (in meters) for different SIZE ranges. The five plots below are histograms of the angle between the telescope axis and the primary particle incident direction (in degrees). In all cases filled histograms contain all* **p** *and* **He** *showers, while the ones with error bars are produced only with those in which more than 70% of the shower light on the camera was produced by muons.*

area, and so a detailed study on it is needed.

5.2 A caveat of the study: distant hadronic showers

One important issue when estimating from the simulation the total rate of hadronic showers, is whether or not all the hadrons which would be able to trigger the telescope in real life have been simulated. For computing speed reasons, one cannot afford generating hadronic showers up to very large impact parameters or with directions too different from that of the telescope axis. The reason is that trigger efficiency would be very low and then a huge number of showers would have to be simulated to achieve the same number of triggered (that is, usable) events. As explained in §2, in our MC **p** and **He** library the maximum impact parameter is 400 m and the maximum off-axis angle is 5 degree. In figure 2 we can see how, for SIZE < 2000 photons, an important part of the hadronic showers have large impact parameters, and many are expected to lie beyond 400 m. On the other hand, the 5 degree seem to be enough to contain most showers. As one would expect, the two quantities are correlated: the average off-axis angle of the triggered showers depends on the impact parameter, but we estimate that 5° should be enough even for i.p. up to 800 m. A "wiser" MC production would make the angular distribution of shower axes depend on the impact point on the ground with respect to the telescope. It is doubtful whether such a production will ever be worth the effort, since once we come to know the instrument well, real data should provide us with loads of background events, and the MC library will become mostly a gamma library.

The main culprit for the lack of "convergence" of MC in impact parameter are showers in which a large part of the light is produced by muons. This is clear by observing, in fig. 2, the histograms made only with these muon dominated showers: at the lowest SIZE bin they constitute half of the background at 400 m impact parameter, for SIZE between 500 and 1000 photons they are about 75%, and, above 1000 photons, distant showers are made up almost exclusively by muons. All this has to be taken into account when interpreting the results in this note, or comparing them to real data. For SIZE < 1000 photons, perhaps half of the background events that we would have in the real telescope are not being considered in this study[4], with the subsequent overestimate of the telescope performance in terms of sensitivity. We cannot simply scale the obtained sensitivities as the square root of the factor by which the background is underestimated, because these distant, muon dominated showers will not be comparable to the rest. Perhaps they are more easily discriminated (through timing?), but at the present point we have no proof of it.

5.3 A correction to TDAS 03-01

In an older work, we stated that the convergence of our MC hadron library was satisfactory (see fig. 3 of [8] - which is **wrong**). The reason was simply that the impact parameter calculated by the camera program (v0.6) was not correct: it was defined as the distance between the telescope axis and the shower axis (in the sense of distance between two straight lines). Obviously, that is not the physically relevant quantity here: what matters is the distance between the telescope position (i.e. the mirror dish center) and the shower axis (distance between a point and a straight line). We have fixed this in camera 0.7. If one reconstructs the impact parameter correctly in the old MC data used in [8], the convergence is roughly as bad as the one seen on figure 2.

6 Results

The resulting integral sensitivity curve for the current MAGIC setup is shown in figure 7. The error bars derive exclusively from the statistical uncertainty of the quality factor (before ALPHA cut), dominated by the low hadron statistics after cuts.

We have also made 10 hour long "virtual observations" of the Crab Nebula, using a realistic gamma ray spectrum[5]. These are shown in figures 8 to 11, where the expected ALPHA distributions for the background (p + He) and photons from the Crab nebula after γ/hadron separation are displayed. Each row of two plots corresponds to a sample with a given lower SIZE cuts (ranging from 0 to 7000 photons). For the Crab, the flux above 1 TeV has been taken from [2], and below 1 TeV we have used the parametrization given in [17] which includes spectral hardening towards lower energies (see fig. 7). The background shown on the right column histograms consists of the actual MC hadronic events surviving the gamma / hadron separation. This gives an idea of the big uncertainties of the residual background estimates at high energies. On the left column, the (fake) residual background after cuts which we would integrate in 10 hours has been generated at random, simply following the straight line fit (blue line) which was performed on the ALPHA distribution of MC hadrons **before**

[4] Of course, "all other things being equal"; for low SIZE values the trigger performance determines the rate, and the simulated trigger may not reproduce the real one in detail. So we may even see lower event rates in the data than shown in this work, but implying also lower gamma rates.

[5] Note that this is rather different from the pure power-law used in the integral sensitivity estimate!

γ/hadron separation (see §4.9). The expected gamma signal from the Crab Nebula is indicated by the red histogram.

6.1 Crab signal in SIZE bins

Figures 8 - 11 show the *integral* excess above a certain SIZE value. It is perhaps more useful to plot the signal in SIZE bins, in a *differential* way. This is what is presented in figures 12 to 14. We have chosen the optimal hadronness cut for each SIZE bin independently, again requiring that at least 50% of gammas survive the cut (except in fig. 13, bottom, see next section). From the plots we see that, under the ideal conditions of MC, a clear signal from Crab would be seen in 10 hours, even at the lowest SIZE bin. The obvious problem is that to achieve that, one needs an extremely unbiased and reliable background: note that for SIZE $<$ 500 photons a systematic error of around 1% in the determination of background at low ALPHA would completely destroy (or double!) the excess. Naturally, for weaker sources the situation would even be worse. Looking at the plot, a simple extrapolation of the ON-source histogram from large ALPHA down to small ALPHA does not look like a good alternative. The situation improves for the second SIZE bin, from 500 to 1000 photons (fig. 12, bottom), thanks to narrower ALPHA for gammas and lower residual background (but then the median energy is already above 80 GeV). Of course the presented analysis is not particularly suited for the smallest showers, and hopefully we will find better methods for background supression. But whatever the method, at the lowest energies we can expect rather small signal to noise ratios even for Crab[6], and we will have to work hard to get a reliable signal. We must not underestimate how important it is to have a good and unbiased background, either from OFF observations or otherwise.

6.2 Tighter separation cuts

From the above discussion, it turns out that, specially for not too weak sources, and low energies, a tighter background discrimination cut may be convenient. This can be the case even if the quality factor is equal or smaller than for a looser cut, because the decrease in significance would be compensated by a higher fraction of gamma showers in the ON region, which in turn would reduce the problem of the possible systematic errors in the determination of background we just discussed. This will not make better the flux sensitivity estimates here presented, since in the MC we have a perfectly unbiased background. But may be an important point when dealing with real data.

In the two lowest SIZE bins and with the current analysis we did not get any significant improvement in this respect by applying tighter cuts to the Crab MC (but this would depend on the strength of the source). In the 1000 to 2000 photons bin, a very tight cut, keeping only 14% of gammas, can be rather useful, as is shown in figure 13. The median energy increases only slightly (by $\simeq$ 10%) due to the tight cut, but the situation regarding the background is much better: for instance it now looks possible to safely extrapolate the background from high to low ALPHA using only the ON data, which on the upper panel of fig. 13 seemed much more risky. The conclusion is that "maximum quality factor" must not be the only guideline to choose the cut value.

6.3 Effect of bad mirror performance

In the first draft of this note we studied different MC mirror setups which represented the telescope in various stages of the comissioning phase. In this version we have concentrated on the study of a single setup, which we believe corresponds to the current real telescope. On top of this, we have also repeated

[6] We expect to find also stronger sources than Crab at these energies

the described analysis on two of the MC samples used for the first draft, the result of which is shown in fig. 19. The lower graph shows the sensitivity obtained for a setup with the same mirror performance we have assumed elsewhere in this work. The upper graph has been obtained calculated with a worse mirror (projected σ of the spot around 0.1° in both axes), all other things being equal. We think that situation corresponds to the telescope performance before the chessboarding and readjustment of mirror panels in August 2004. Figure 19 shows the importance of keeping the spot small. The bottom plot shows roughly the same sensitivity of fig. 7, although they are not identical because there are slight differences in the used simulation (higher light collection efficiency and no FADC clock noise). In contrast, the upper plot shows an increase of up to a factor 2 (depending on E) in the minimum observable flux, or in other terms, it would increase the necessary observation time for a given source by a factor of 4.

7 Discussion

In this work we have used the kind of analysis most people is currently applying to our real data (image parametrization in moments up to third order). The results show that the analysis works quite well for SIZE $>$ 1000 photons, achieving background supression factors above 50, while keeping half of the gammas or more (before ALPHA cut), as can be seen in tables 3 and 4.

7.1 γ / hadron separation at low energies

At lower SIZE values, the discrimination which is possible with these parameters is very poor, since the parameter distributions for gammas and hadrons greatly overlap each other (see fig. 15 and top of fig. 16). Note also that even one parameter, CONC, at low SIZE shows the opposite behavior as usually expected: hadron showers are more concentrated than gamma ones (perhaps due to the large number of single muons[7]). We see therefore that the reason for the bad performance of the analysis is not a malfunctioning of the classification method employed (random forest), which on the other hand seems to work extremely well: in fig. 17 we see the case for the SIZE bin 2000 to 4000 photons, and from the distributions of image parameters after the hadronness cut it seems quite obvious that no further separation using the same parameters is feasible.

In the output of Random Forest low SIZE showers show up as the large number of events, both gammas and hadrons, with intermediate hadronness values (see fig. 3). This population decreases rapidly as the SIZE cut increases. A more detailed analysis indicates that, for what regards to WIDTH and LENGTH, the problem is one of pixelization. For SIZE $<$ 1000 photons the WIDTH distribution peaks at around half the diameter of an inner pixel, both for gammas and for hadrons (and the shape of the distribution is about the same). The LENGTH distribution peaks at somewhere between 20 and 25 mm (less than the inner pixel diameter), and is also rather similar for gammas and hadrons. The distributions of the scaled versions of WIDTH and LENGTH for low SIZE can be seen if figures 15 and 16 (top). This means that these parameters (which are the most useful ones at higher energies) will be of no help in the γ/hadron separation at low energy, at least with the current pixelization. We are not suggesting here that the gamma and hadron distributions would look different on a higher resolution camera: perhaps at low E the showers become intrinsecally more similar (for instance because it may become more likely that we see only a single electromagnetic subshower from a hadronic shower).

[7]The number of muon-dominated showers (see fig. 2) is now larger than reported in previous studies [8], the reason being the more realistic simulation of the telescope optics: now a higher fraction of distant muons manage to shine over 4 pixels and trigger.

7.2 The background problem at low energies

In the very ideal conditions of Monte Carlo, where the background is well known, it is still possible to have relatively good sensitivity below 100 GeV. As we mentioned, however, a problem will appear in real data, because the low hadron supression will imply the need for a very good estimate of the background in the signal region (since a very small relative error could destroy a signal or create a fake one). Unfortunately, it is difficult to find OFF regions completely equivalent to the ON one, and on top of this we must add the problem of varying weather conditions. A fit to the ALPHA distribution of the ON data will suffer from the same problems (see top of fig. 12). Keep in mind that the shown virtual observation examples are for the Crab nebula. When dealing with weak sources the problem will appear even for SIZE cuts higher than 1000 photons.

A good alternative may be to do observations in wobble mode [25], eliminating the need for OFF observations. We have already started a dedicated MC study on this to determine the advantages and disadvatages it will bring. For instance, at the lowest energies, due to limited angular resolution, the method may not work, or work badly. But in my opinion, at least above 100 GeV, and for weak sources, it can be quite useful.

7.3 How can we improve the telescope sensitivity?

Despite the efforts we have made to make the MC as similar as possible to real data, there are a few idealizations which will probably make the real telescope sensitivity worse than predicted here. And in fact, all the analyzed (real) Crab data circulated so far (including those produced with an analysis method similar to the one used by us [16]) result in lower sensitivity than that of fig. 7. Numbers for comparison can be easily drawn from tables 3 to 5. Among the Monte Carlo *idealizations* of the telescope we can cite the following:

- In MC, all inner pixels have the same (constant) average gain, as well as all outer pixels. The relative calibration factor between inner and outer pixels is perfectly known. The electronic chain is linear. No faulty pixels were simulated.
- Ratio of high to low gain is exactly known in MC, and the same (10.0) for all pixels.
- MC Low gain pulses have the same shape of high gain pulses, being hence well contained in the FADC. Besides, in the real data we see larger time jitter, due to trigger or whatever, than we have currently implemented in MC (± 0.5 FADC slices), and so some pulses get integrated only partially.
- We have used no stars in our simulation, just diffuse NSB over the whole camera, corresponding to a dark patch of sky.
- The Monte Carlo trigger has perfect synchronization among all pixels, and identical discriminator threshold for all of them.
- At low SIZE, we have neglected a rather large fraction of the hadronic background: showers with impact parameter larger than 400 m (see §5.2)

Therefore, the sensitivity estimated in this MC study **cannot** be improved by:

- Making better calibration routines for the real data, for instance with the use of interleaved calibration events, or doing an intensity calibration to detect and correct nonlinearities: this will make the data look more like the Monte Carlo, but can not lead to better sensitivity since we have assumed a perfect intercalibration of pixels and perfect linearity of their response. The same applies to better treatment of low gain. We should rather expect a worsening of our current estimate, once we implement all these features more realistically in the simulation.

- Reducing the integration window to catch less noise. Since the simulated noise level is rather low, and we introduced no stars, we see in table 2 that the intrinsic poissonian fluctuations of the smallest Cherenkov signals surviving cleaning (which are around 4 phe$^-$ for pixels in the inner camera) are roughly equal to the NSB fluctuations ($\sigma \simeq 2$ phe$^-$). For increasingly large signals, the NSB fluctuations become smaller and smaller compared to the signal fluctuations, and hence you cannot expect a very big gain from reducing the integration window. We do not refer only to adding up less FADC slices. A preliminary study using a special simulation with 2 GSample FADC (and single phe$^-$ response half as wide as the current one), in which we integrated only 5 instead of 20 ns, showed no visible difference in sensitivity. In connection to this, I think the term "image cleaning" is a bit misleading because it seems to imply that the goal is simply to remove pixels with only NSB and no Cherenkov photons. "Tail cut" is a more appropriate name, since even in the case of running the simulation with no noise at all, the pixels with very small signals must be rejected before calculating moments, in order to achieve a decent discrimination. Of course, in real conditions (higher diffuse NSB and stars in the FOV), the reduction of the integration time which will be possible with the future FADCs will have a positive effect on the real telescope performance, but again, in the sense of bringing it closer to the MC estimate than it is now. Also, the use of more sophisticated analysis methods (other than moment calculations) may benefit from lower noise, if they are able to use in some way also pixels with very small signals. So, the somewhat pessimistic statement above regards only the type of moment analysis we have done up to now.

- Improving the performance of the real MAGIC L1 trigger (synchronization of channels, tuning of discriminator thresholds, etc).

The sensitivity might be improved in one of the following ways:

- Adding a second telescope to work in stereoscopic mode. Our studies in this respect [19] show that a gain in sensitivity of up to a factor 2 is achievable. Not only sensitivity, but also angular resolution and energy resolution will become better with stereoscopic analysis, although the latter improvement still has to be quantified for the particular case of MAGIC vs. MAGIC-2. Better angular resolution will also make wobble mode easier, allowing to define more OFF regions on the camera.

- New analysis methods: new parameters, methods based in other than image moments (like the so called *model analysis*), use of timing... We must say however that to our knowledge no analysis method which results in a significative improvement in performance has yet been tried succesfully on the MAGIC Monte Carlo. There is much speculation regarding, for instance, timing, but we have no clue of by how much it will help in the analysis, nor with the current FADCs neither with the future faster systems. The fact that the distribution of arrival times at ground of Cherenkov photons from hadron and gamma showers differ on a large scale (hundreds of meters), does not mean that the differences we can measure with a 17 m Ø reflector will be of any help. Even if there are measurable differences, they have to be independent of the parameters we have already used, in order to improve our sensitivity. In other words, we need methods to identify gamma-like hadrons, those surviving our current cuts, and this is obviously a much harder task. Thorough studies are needed on image timing, specially for the future FADCs.

7.4 Increasing the light collection

One of the possible upgrades of the telescope consists in the use of high quantum efficiency photodetectors. We have already used QE vs λ curves from such devices in the simulations made for MAGIC-2 [19] and ECO-1000 studies [6]. The main advantage of enhancing the light collection efficiency of the instrument, no matter whether through better photodetectors or through the use of a larger mirror, is obviously a lowering of the energy threshold. However, our studies show that the improvement in sensitivity, at energies above the threshold of the smaller (or less efficient) telescope, is rather marginal. Again, we are referring to the kind of moment analysis we have tried. It is not so surprising that at a given energy the γ / hadron discrimination does not improve by collecting more photons. We do certainly reduce the (relative) fluctuations of the registered signals, but this does not automatically translate in better separation: we may well be limited by intrinsic shower fluctuations, and therefore gain little by collecting photons in a larger area around the same position on the ground. Besides, the collection area is in any case much smaller than the total Cherenkov light pool. By collecting more light in the same area, we will have roughly the same ahower image on the camera as before, just brighter against the NSB fluctuations (see above). It is therefore quite natural that for showers large enough as to be “bright” in a “small” telescope the image parameters as seen on a “large” telescope will change little, and consequently discrimination will be about the same. This is what we have seen in the above mentioned studies. Of course, using (hypothetical) analysis methods which make use of image tails, there may be a gain in sensitivity at all energies, but this has yet to be proved. In the particular case of hadron showers of which the telescope sees a single electromagnetic subshower[8], collecting more photons around the same point in the ground will not change anything at all. Having a telescope in another location is more helpful since it can image a different part of the hadronic shower.

As a conclusion, to gain in sensitivity at a fixed energy, our current knowledge suggests that the safest way is the use of more than one telescope. To go down in threshold, we obviously need better light collection. But we should always keep in mind that we lack an efficient analysis even at the current near-threshold energies of MAGIC. It should be investigated whether alternative analysis methods can be found at those and lower energies, otherwise the problem of background determination discussed in §7.2 will be worse than it is now in MAGIC, and it might be impossible to get any reliable signal at all.

[8]We do not know what the rate of these are; it is an interesting issue somebody should address.

BEFORE TRIGGER							
Produced MC showers	train	$N_{\gamma,\mathrm{prod}}$	3.9	$N_{\mathrm{p,prod}}$	13.0	$N_{\mathrm{He,prod}}$	6.5
$E_\gamma > 10$ GeV, $E_{\mathrm{p,He}} > 30$ GeV	test	$\times 10^6$	3.9	$\times 10^6$	13.0	$\times 10^6$	6.5

AFTER CLEANING AND IMAGE PARAMETRIZATION ($\geqslant 3$ pixels)							
SIZE $>$ (photons)	0	300	500	750	1000	1500	1999
$N_{\gamma,\mathrm{train}}$ (reduced)	16767	14207	10621	7384	5531	3559	2586
$N_{\mathrm{h,train}}$	11175	9629	7243	5087	3815	2478	1785
$N_{\gamma,\mathrm{test}}$	120170	84629	55277	36020	25955	16242	11497
$N_{\mathrm{h,test}}$	11300	9600	7263	5074	3796	2541	1873
E_0 (GeV)	36.5	52.8	71.5	97.0	130.7	170.1	221.5
Proton rate (Hz)	195.8	165.8	123.8	84.8	62.6	41.1	30.0
Helium rate (Hz)	53.4	46.1	36.8	27.8	21.8	15.6	11.8
p + He rate (Hz)	249.2	211.8	160.6	112.6	84.4	56.7	41.8
AFTER γ/hadron separation (without ALPHA)							
Hadronness $<$	0.456	0.367	0.271	0.175	0.0963	0.0539	0.0500
Q-factor	1.35	1.50	1.75	2.35	3.44	4.72	5.62
$N_{\gamma,\mathrm{test}}$	96121	59235	33165	18008	12976	9743	8042
$N_{\mathrm{h,test}}$	3968	2078	855	230	80	41	29
ε_γ	0.80	0.70	0.60	0.50	0.50	0.60	0.70
ε_{h}	0.351	0.216	0.118	0.0453	0.0211	0.0161	0.0155
p + He rate (Hz)	87.5	45.9	18.9	5.10	1.78	0.91	0.65
AFTER ALPHA cut							
$\lvert$ALPHA$\rvert < (^\circ)$	13.75	10.25	8.375	5.75	5.125	5.125	5.125
$N_{\gamma,\mathrm{test}}$	56022	36841	22149	11761	8563	6846	5995
$N_{\mathrm{h,test}}$ (estimated)	626.6	245.6	82.9	15.6	5.00	2.62	1.81
Q-factor enhancement	1.47	1.81	2.14	2.51	2.64	2.78	2.97
Total Q-factor	1.98	2.72	3.75	5.88	9.08	13.1	16.7
Total ε_γ	0.466	0.435	0.401	0.327	0.330	0.422	0.518
Total ε_{h} ($\times 10^{-2}$)	5.54	2.56	1.14	0.308	0.132	0.103	0.0965
p + He rate = R_{h} (Hz)	13.8	5.42	1.83	0.347	0.111	0.0585	0.0404
E_0 (GeV)	46.2	57.2	70.5	120.4	154.0	187.4	225.6
$\Phi_{E>E_0}$ ($\times 10^{-11}$ cm^{-2} s^{-1}) Min. flux, 5 σ in 50 h	9.32	6.31	4.37	1.52	0.797	0.528	0.374
N_γ in 50 h from min. flux	7884	4938	2872	1249	708	513	426
N_γ in 10 h from Crab	16250	12293	8730	5552	4377	3657	3319

Table 3: *Calculation of the integral flux sensitivity of MAGIC for point sources, summary of relevant numbers for lower SIZE cuts up to 1999 photons. The subscript h refers always to MC hadrons, that is, protons and Helium nuclei. E_0 is the peak energy for gammas, given the original spectrum $dN/dE \propto E^{-2.6}$*

BEFORE TRIGGER						
Produced MC showers	train	$N_{\gamma,\mathrm{prod}}$	3.9	$N_{p,\mathrm{prod}}$	2.6	No He
$E_\gamma > 10$ GeV, $E_p > 200$ GeV	test	$\times 10^6$	3.9	$\times 10^6$	2.6	events

AFTER CLEANING AND IMAGE PARAMETRIZATION ($\geqslant$ 3 pixels)						
SIZE > (photons)	2000	3000	4000	5000	6000	7000
$N_{\gamma,\mathrm{train}}$ (reduced)	6218	3911	2732	2056	1652	1345
$N_{h,\mathrm{train}}$	6484	4343	3217	2540	2085	1734
$N_{\gamma,\mathrm{test}}$	11494	6951	4803	3588	2821	2278
$N_{h,\mathrm{test}}$	6450	4266	3098	2460	2045	1692
E_0 (GeV)	221.5	287.3	360.0	452.4	510.6	566.6
Estimated $\frac{\text{p rate, E<200 GeV}}{\text{p rate, E>200 GeV}}$	0.14	0.07	0.03	0.01	0.00	0.00
Proton rate (Hz)	28.2	17.5	12.2	9.5	7.8	6.5
Helium rate (Hz)	Estimated as 40% of proton rate					
p + He rate (Hz)	39.5	24.5	17.1	13.3	11.0	9.1
AFTER γ/hadron separation (without ALPHA)						
Hadronness <	0.0483	0.0540	0.0962	0.0838	0.0689	0.0732
Q-factor	5.93	7.72	8.90	10.24	12.05	12.44
$N_{\gamma,\mathrm{test}}$	6895	4864	3842	2870	2256	1822
$N_{h,\mathrm{test}}$	66	35	25	15	9	7
ε_γ	0.60	0.70	0.80	0.80	0.80	0.80
ε_h ($\times 10^{-2}$)	1.02	0.820	0.807	0.610	0.440	0.414
p + He rate (Hz)	0.404	0.201	0.138	0.0813	0.0483	0.0376
AFTER ALPHA cut						
|ALPHA| < (°)	5.125	5.0	5.0	5.0	5.0	5.0
$N_{\gamma,\mathrm{test}}$	5232	3945	3231	2485	1970	1613
$N_{h,\mathrm{test}}$ (estimated)	4.32	2.25	1.59	0.92	0.55	0.42
Q-factor enhancement	2.97	3.20	3.34	3.49	3.54	3.60
Total Q-factor	17.6	24.7	29.7	35.8	42.7	44.7
Total ε_γ	0.455	0.568	0.673	0.693	0.699	0.708
Total ε_h ($\times 10^{-4}$)	6.69	5.27	5.13	3.75	2.68	2.51
p + He rate = R_h (Hz)	0.026	0.013	0.0088	0.0050	0.0029	0.0023
E_0 (GeV)	232.5	302.5	386.5	450.9	500.9	595.2
$\Phi_{E>E_0}$ ($\times 10^{-12}$ cm^{-2} s^{-1}) Min. flux, 5 σ in 50 h	3.29	2.00	1.36	1.04	0.85	0.70
N_γ in 50 h from min. flux	345	241	199	150	115	101
N_γ in 10 h from Crab	2910	2366	2040	1619	1313	1094

Table 4: *Calculation of the integral flux sensitivity of MAGIC for point sources, summary of relevant numbers for lower SIZE cuts from 2000 to 7000 photons. The subscript h refers always to MC hadrons, that is, protons and Helium nuclei. For these SIZE cuts we have used the high energy MC, with protons only above 200 GeV. For calculations the contribution of Helium has been estimated to be a 40% of that of protons. The amount of protons below 200 GeV has also been estimated using the lower energy sample.*

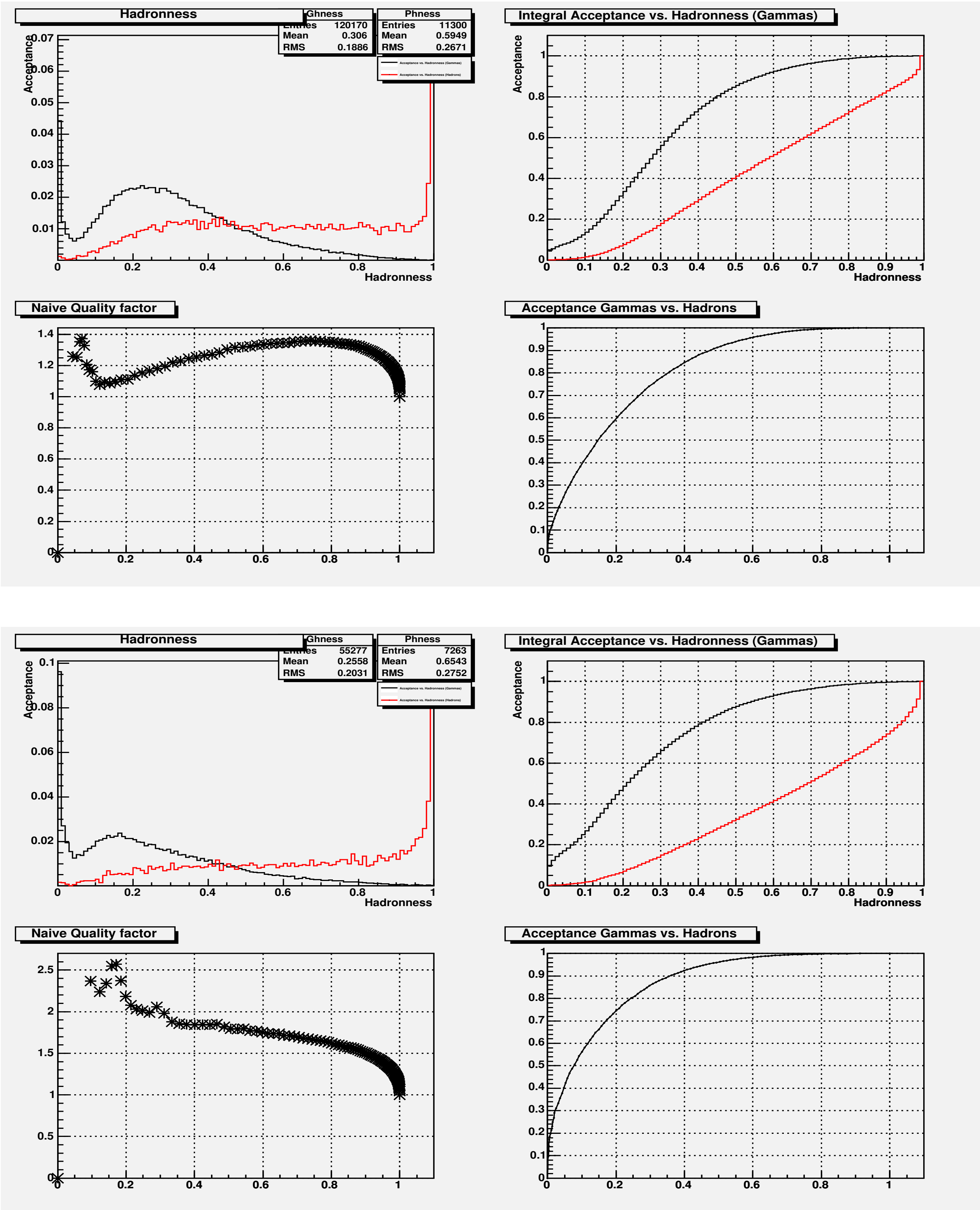

Figure 3: *Output of Random Forest. Top 4 plots: SIZE* > 0*. Bottom 4 plots: SIZE* > 500 *photons.*

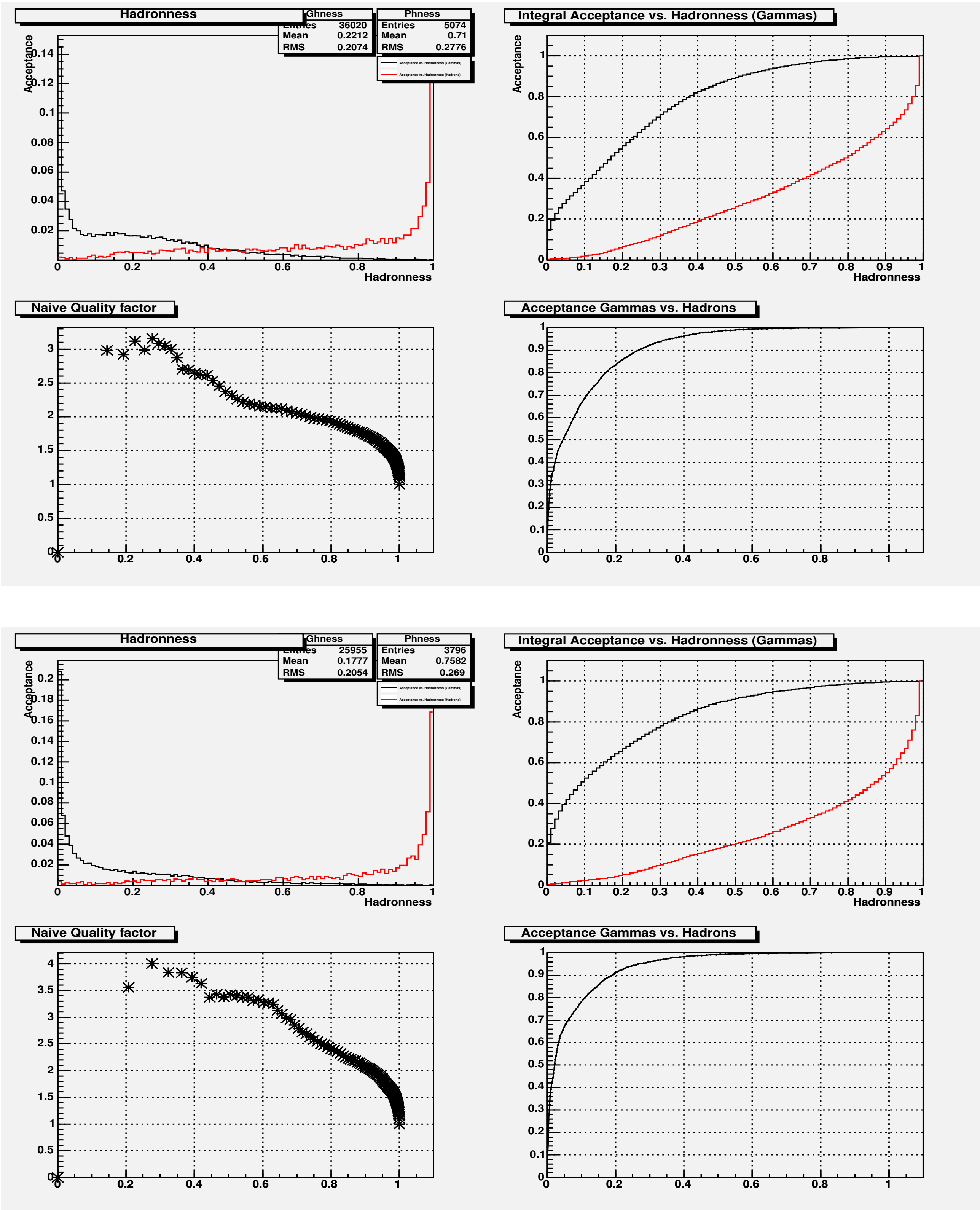

Figure 4: *Output of Random Forest. Top 4 plots: SIZE* > 750 *photons. Bottom 4 plots: SIZE* > 1000 *photons.*

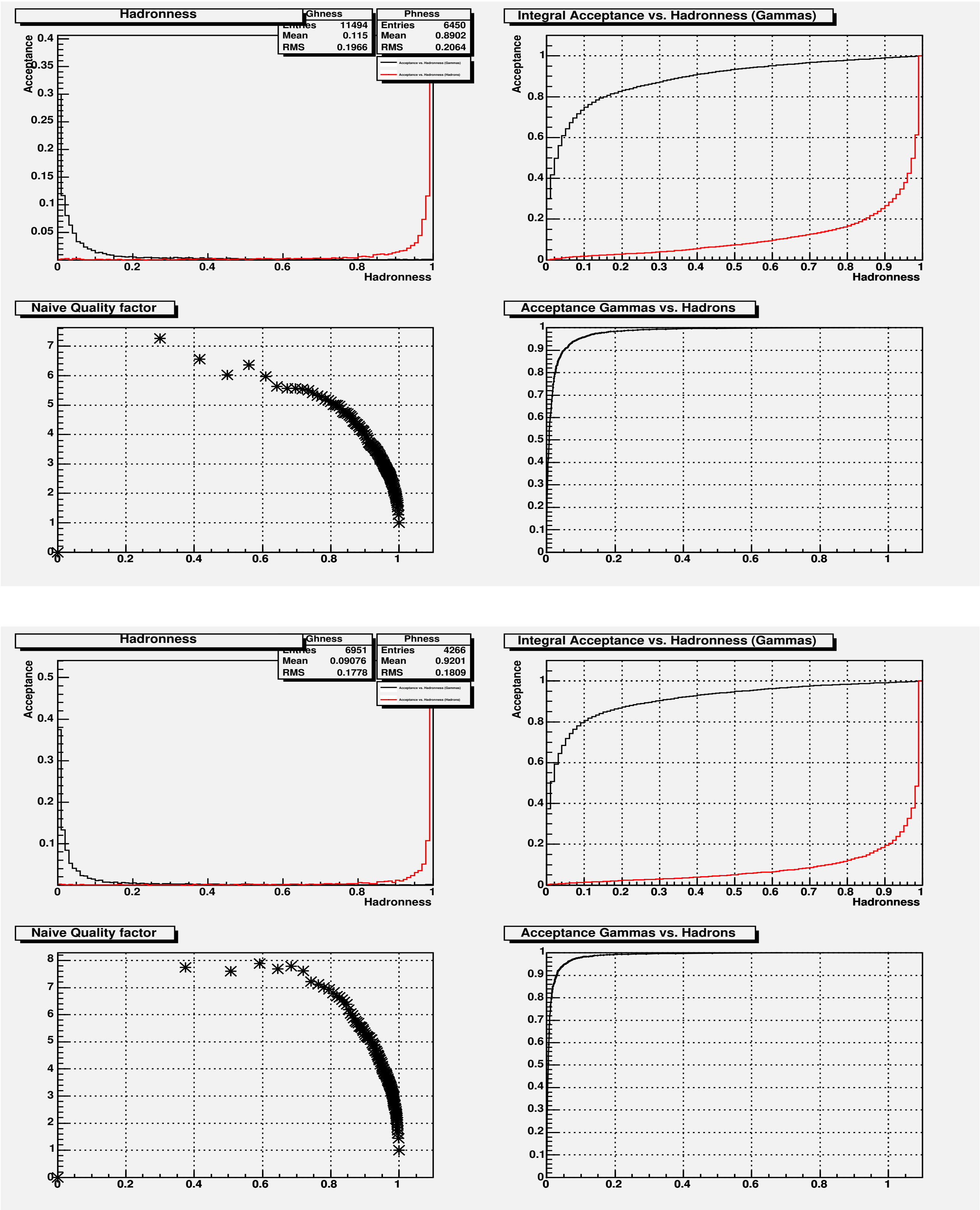

Figure 5: *Output of Random Forest. Top 4 plots: SIZE* $>$ 2000 *photons. Bottom 4 plots: SIZE* $>$ 3000 *photons.*

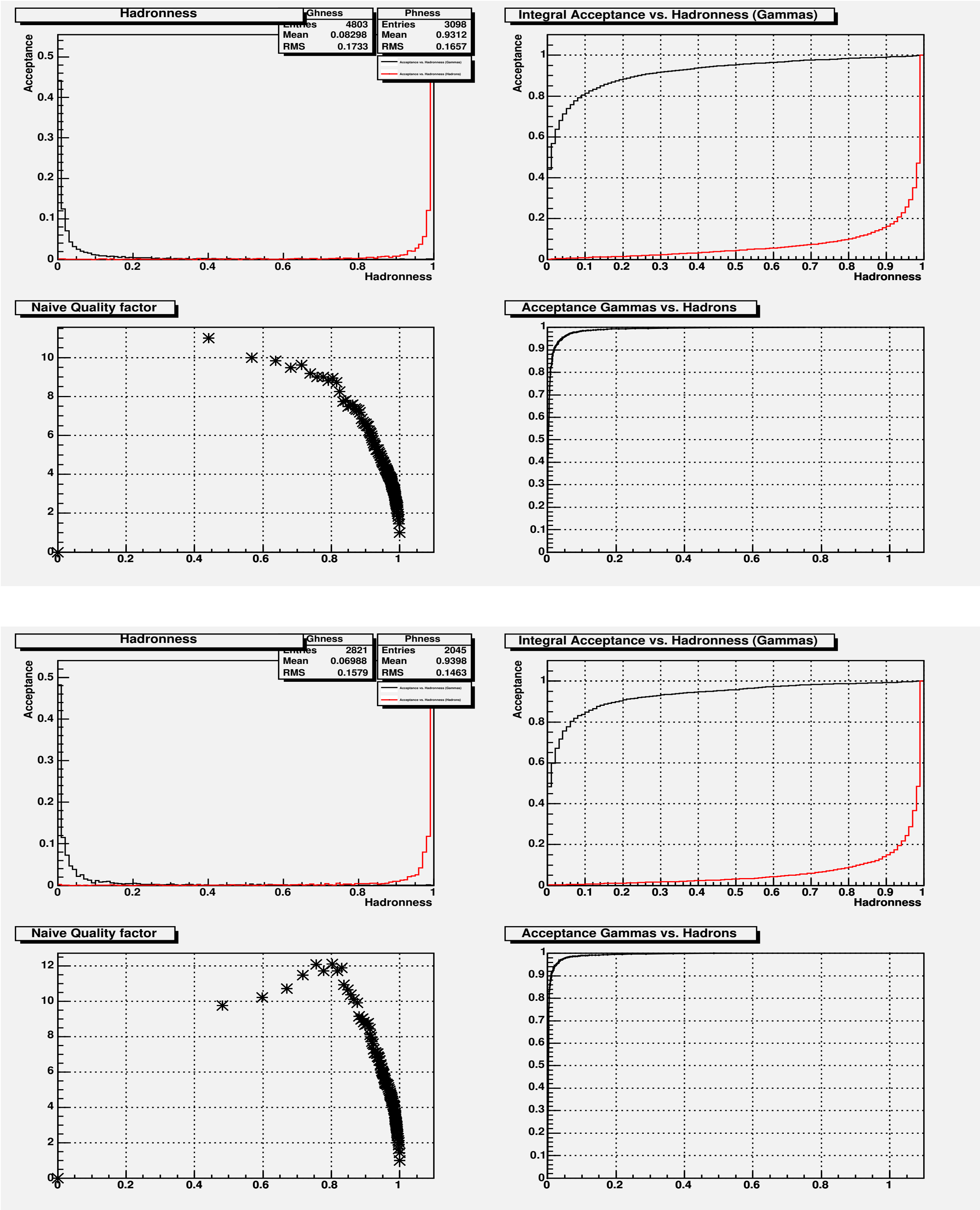

Figure 6: *Output of Random Forest. Top 4 plots: SIZE* > 4000*. Bottom 4 plots: SIZE* > 6000 *photons.*

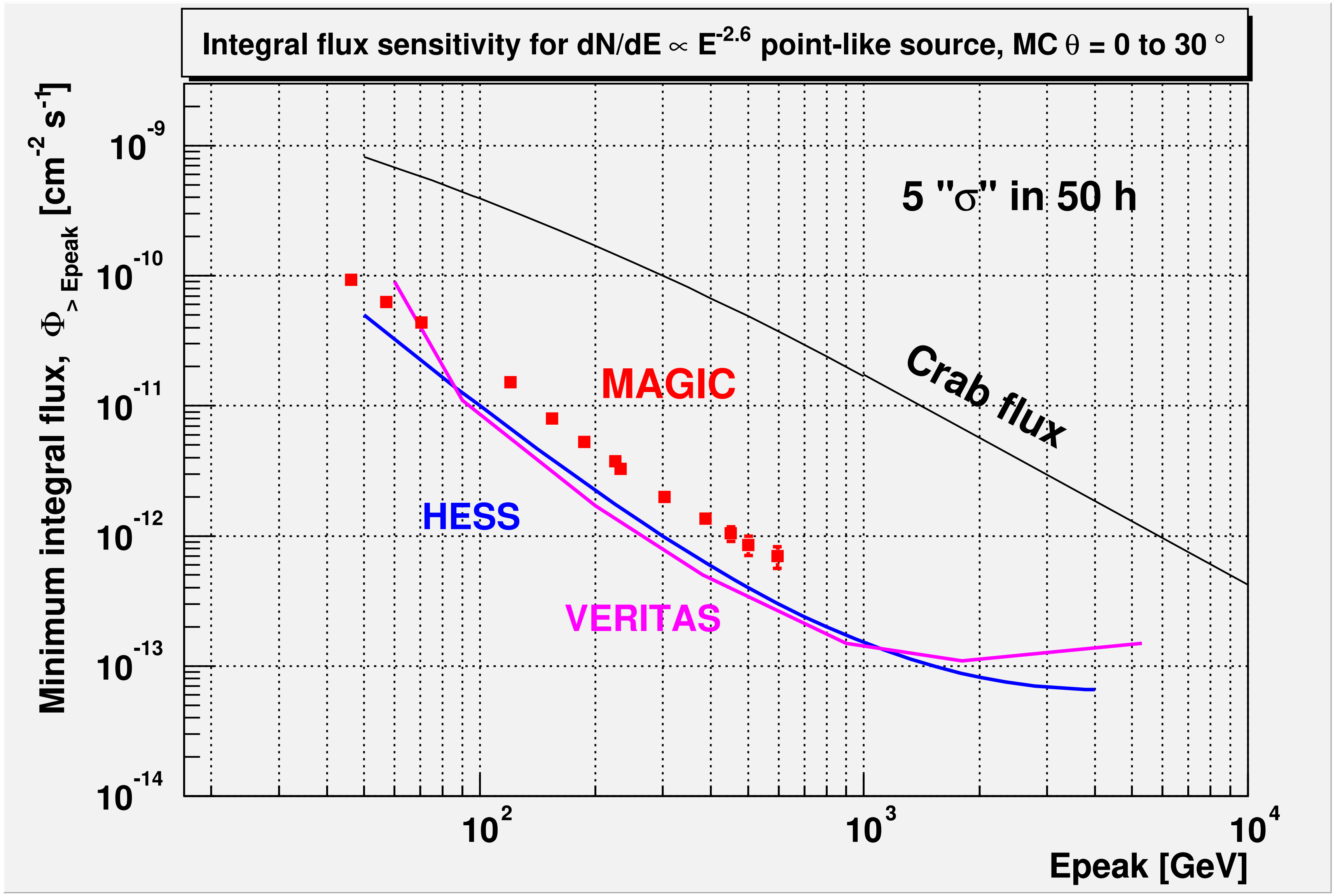

Figure 7: *Integral flux sensitivity of MAGIC, assuming a PSF with projected* σ *around* $0.041°$*. The curves for HESS (4-telescope setup) and VERITAS (7-telescope setup) are taken from [14] and [23]. Of course MAGIC will be able to observe above 600 GeV, the estimate of sensitivity was simply not possible due to lack of MC hadron statistics. Crab flux comes from [2] and [17]. Note that the minimum fluxes on the y-axis refer to a hypothetical source with a pure power-law* $E^{-2.6}$ *differential energy spectrum, not to a source with a Crab-like spectral shape.*

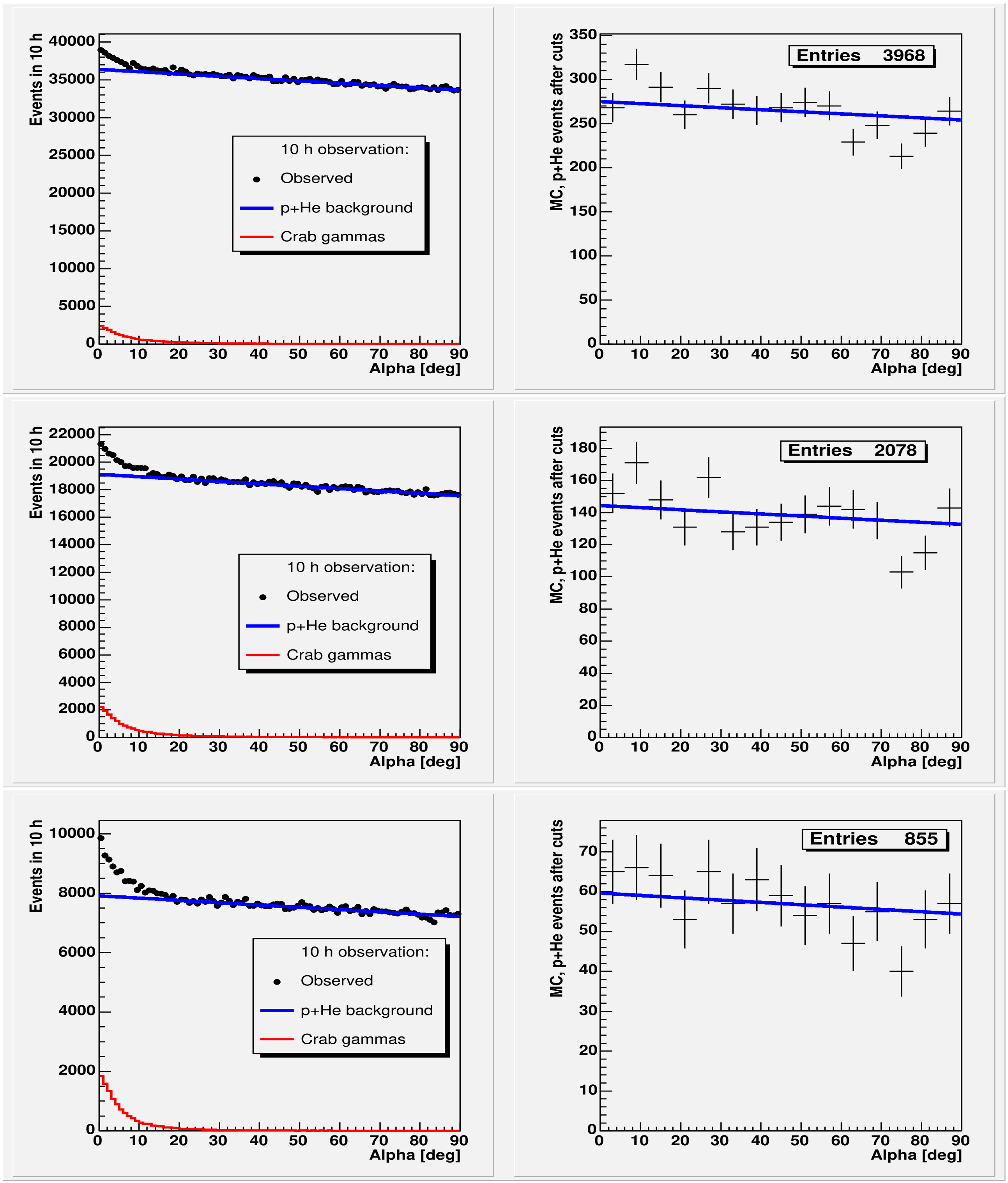

Figure 8: *Right column: ALPHA distributions for the residual background MC events after gamma / hadron discrimination. Left column: ALPHA distribution in a 10 hour virtual observation of the Crab Nebula. The shape of the background (p + He) has been approximated by a straight line (shown in blue) obtained from a fit to MC hadrons before γ/hadron separation cuts (see text). From top to bottom, SIZE cuts > 0, > 300 and > 500 photons, which correspond to gamma peak energies of 46, 57 and 70 GeV.*

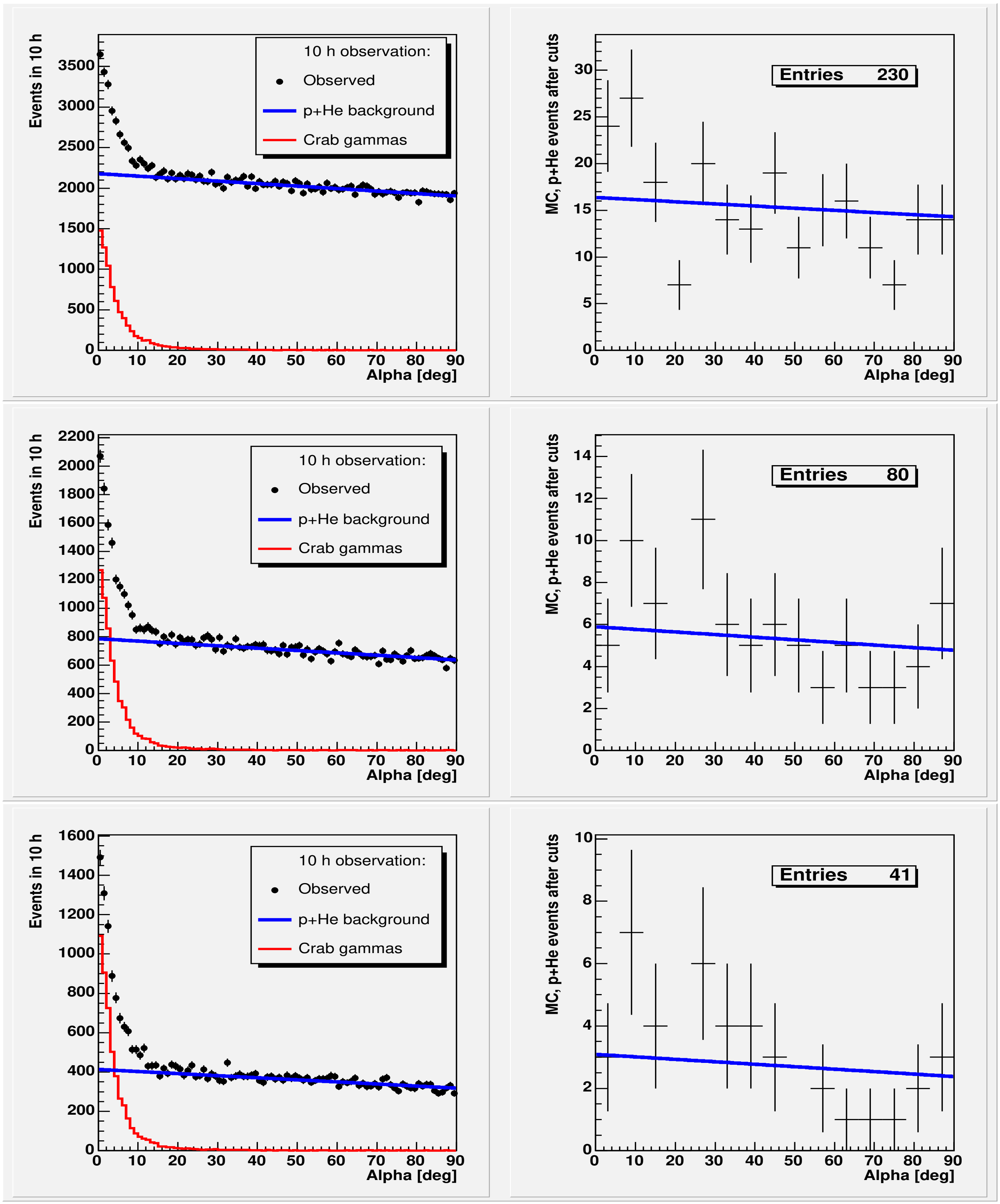

Figure 9: *Same as fig. 8, for SIZE cuts (top to bottom) > 750, 1000 and 1500 photons (peak energies 120, 154 and 187 GeV).*

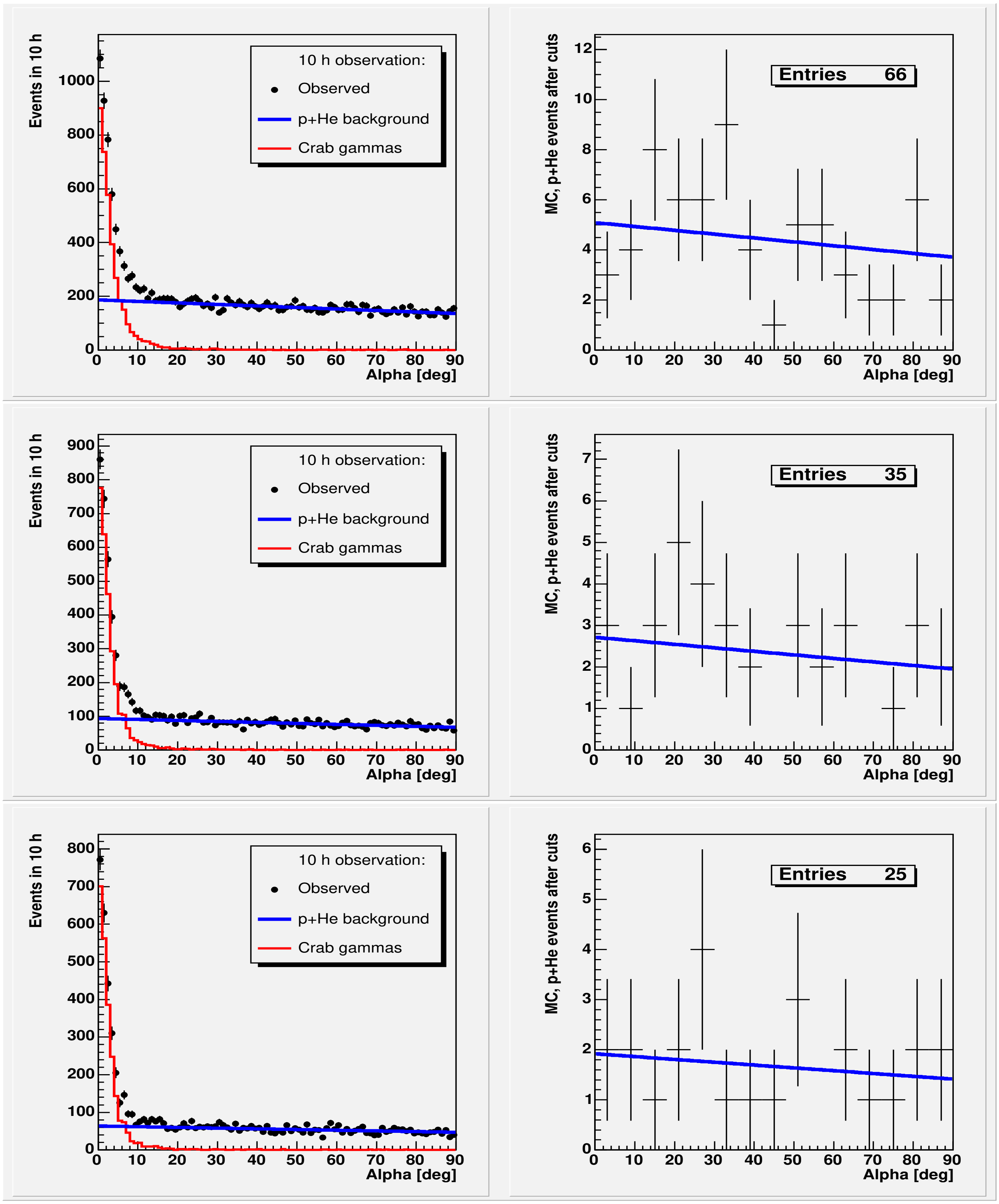

Figure 10: *Same as fig. 8, for SIZE cuts (top to bottom) > 2000, 3000 and 4000 photons (gamma peak energies 233, 303 and 387 GeV).*

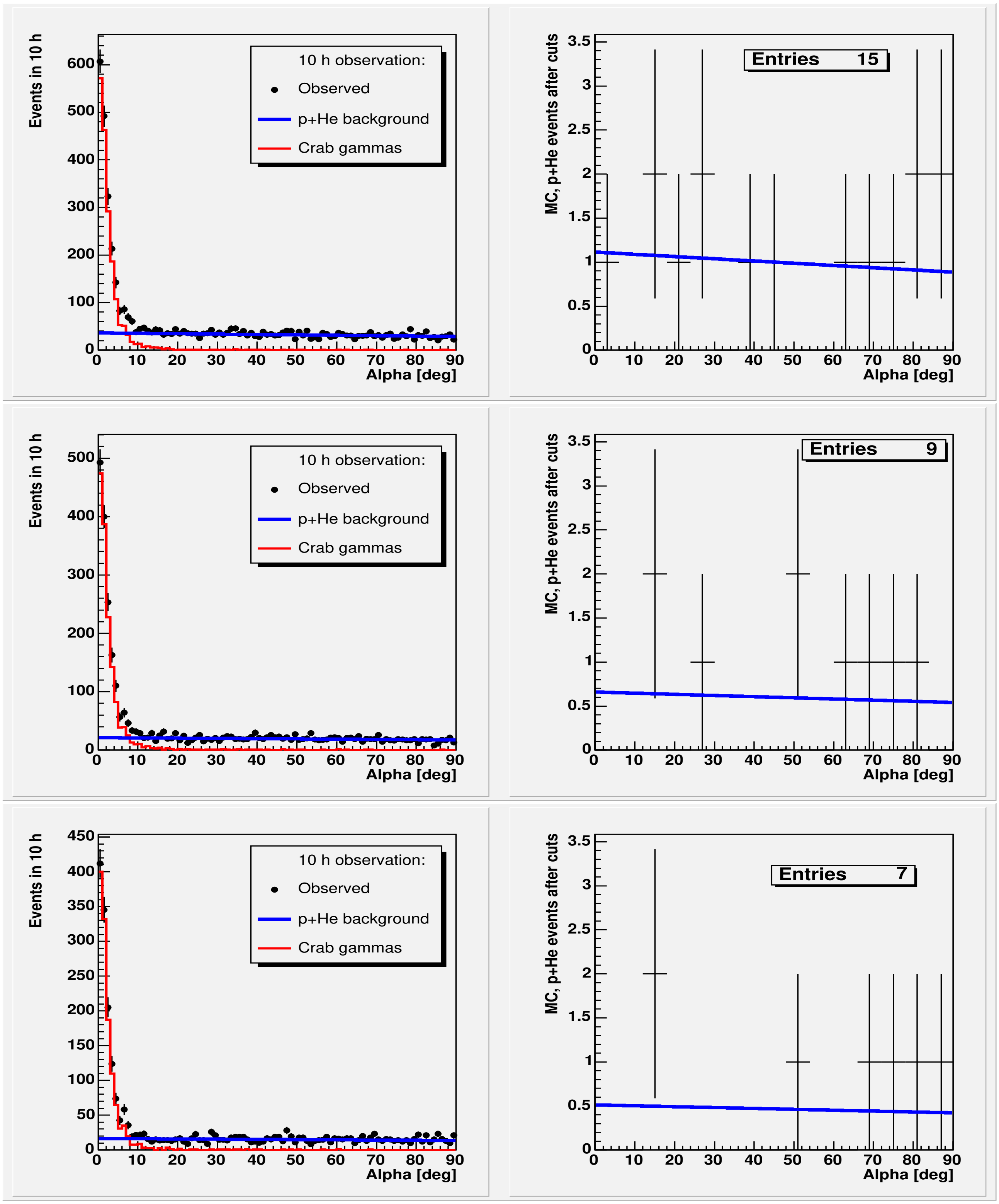

Figure 11: *Same as fig. 8, for SIZE cuts (top to bottom) > 5000, 6000 and 7000 photons, corresponding to gamma peak energies of 451, 501 and 595 GeV).*

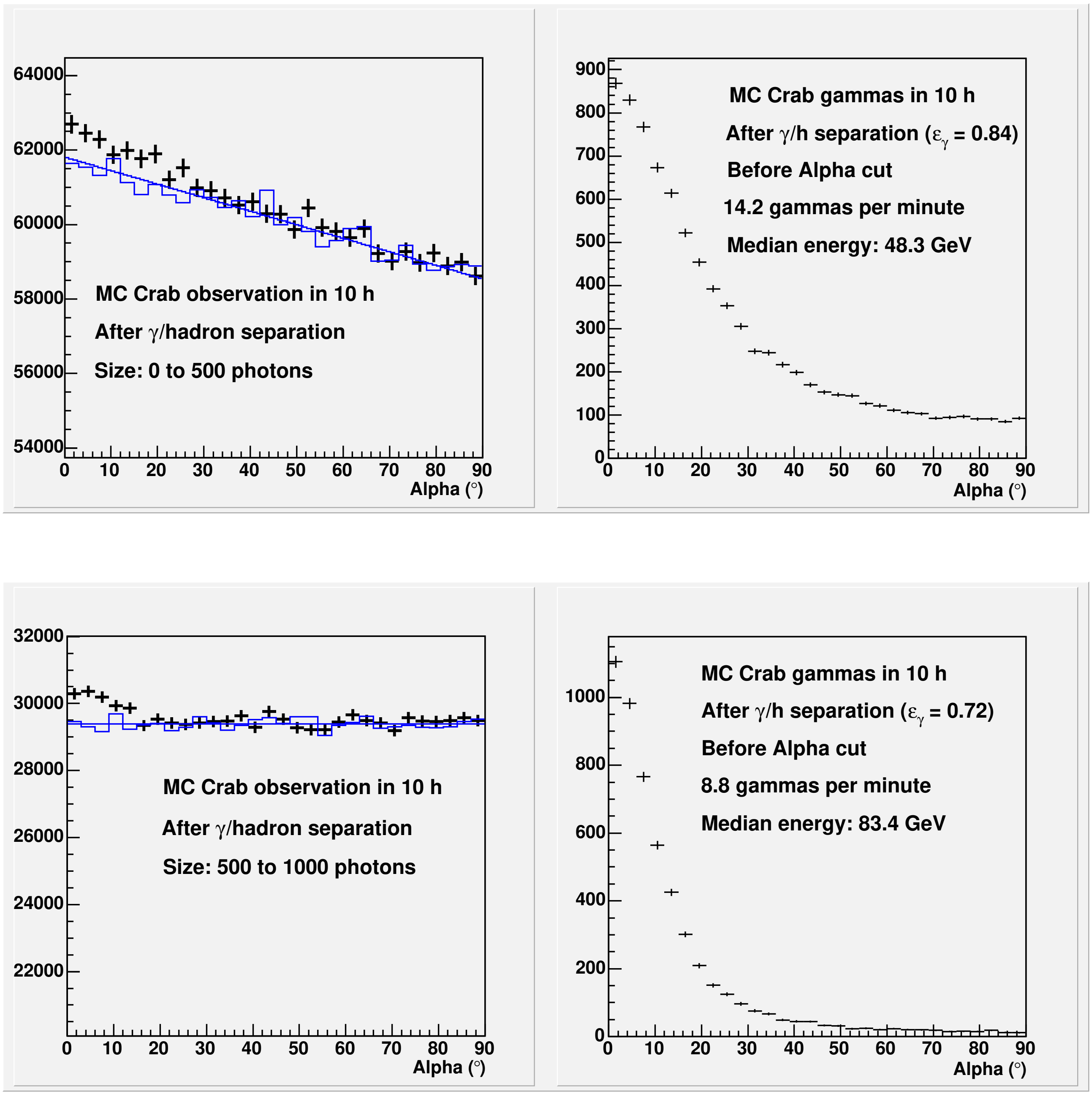

Figure 12: *10 hour virtual observation of the Crab Nebula in different ranges of SIZE. Note that the apparently strong slope of ALPHA in the upper plot is just an artifact of the y-axis scale, expanded to better show the tiny excess.*

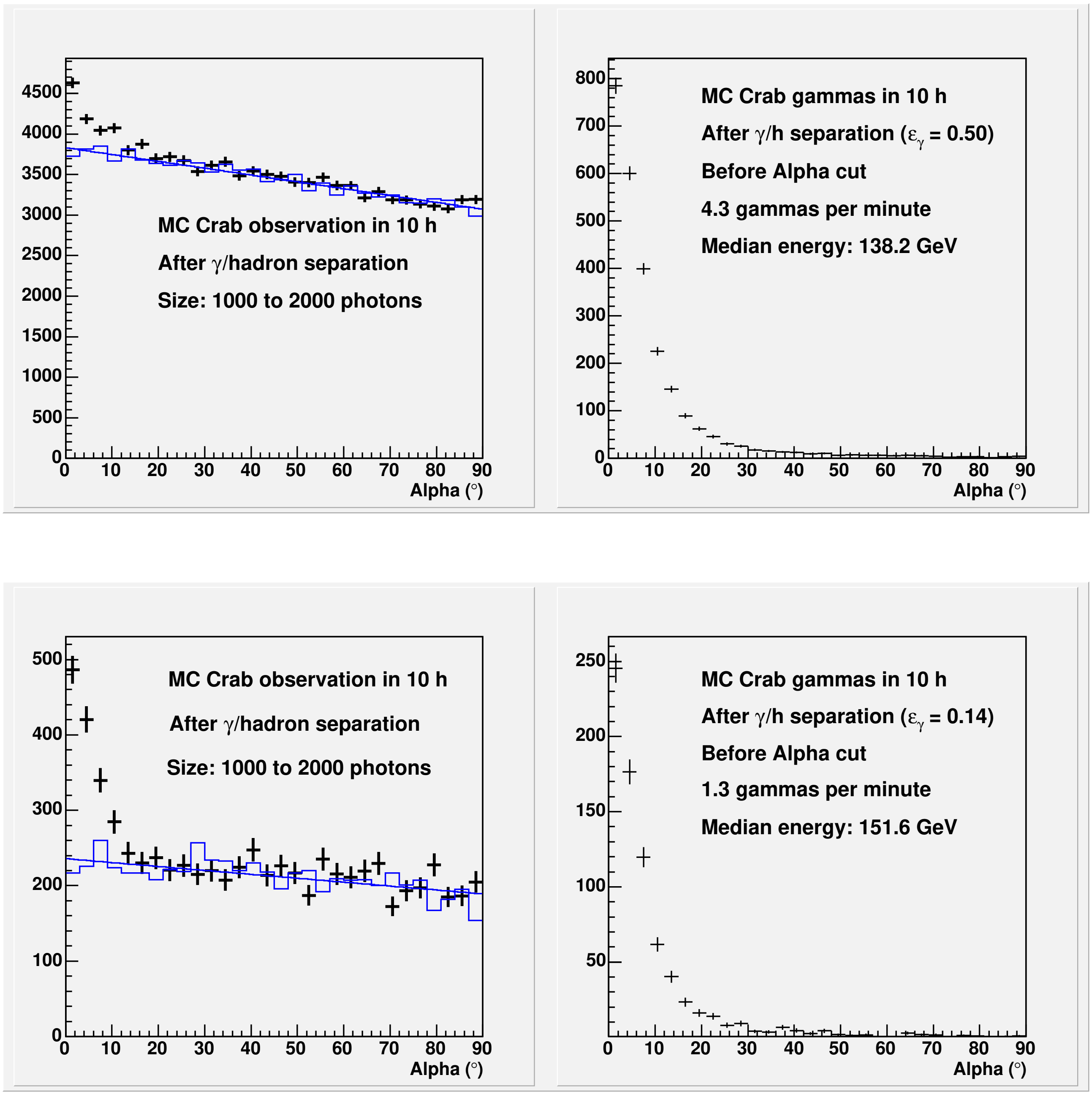

Figure 13: *10 hour virtual observation of the Crab Nebula in the SIZE range 1000 to 2000 photons, with a loose background supression (top), and with a tight cut (bottom) which keeps only 14% of gammas.*

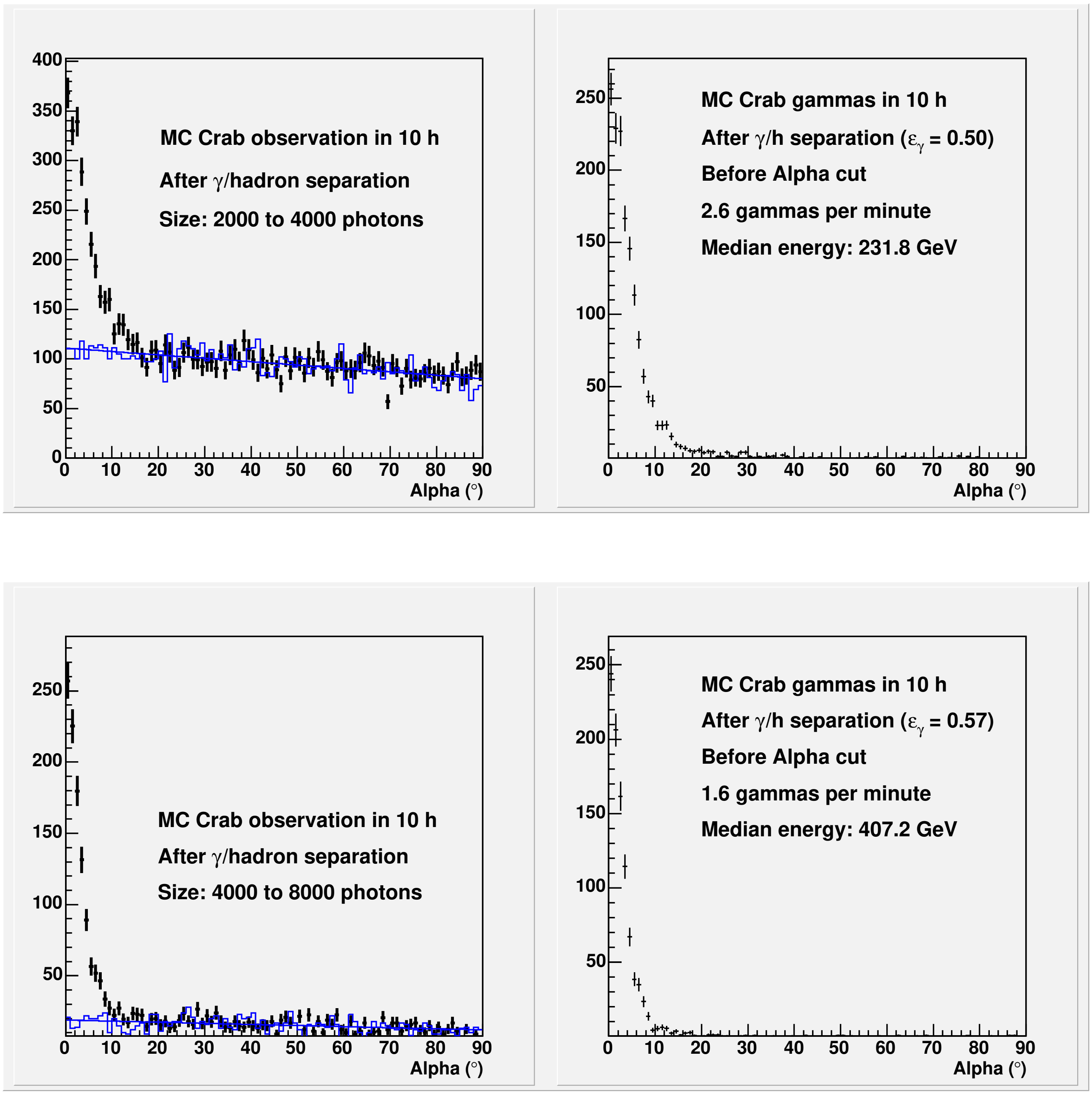

Figure 14: *10 hour virtual observation of the Crab Nebula in the SIZE ranges 2000 to 4000 (top) and 4000 to 8000 photons (bottom).*

SIZE range (photons)	from 0 to 500	from 500 to 1000	from 1000 to 2000		from 2000 to 4000	from 4000 to 8000
Proton rate (Hz)	71.9	61.2	32.7		14.7	6.5
Helium rate (Hz)	16.6	15.0	9.9		5.9	2.6
He + p rate (Hz)	88.5	76.2	42.6		20.6	9.1
AFTER γ/hadron separation (without ALPHA)						
			default cut	tight cut		
Hadronness <	0.516	0.406	0.202	0.0442	0.0418	0.0227
ε_γ	0.84	0.72	0.50	0.14	0.50	0.57
ε_h	0.566	0.321	0.0676	0.00416	0.0116	0.00423
Q - factor	1.12	1.27	1.92	2.17	4.64	8.76
Median E_γ (GeV)	48.3	83.4	138.2	151.6	231.8	407.2
Events in 10 h Crab observation, before ALPHA cut						
N_γ/10 h	8510	5300	2550	752	1552	953
N_h/10 h	1.81×10^6	881.6×10^3	103.6×10^3	6374	8591	1393
Events in 10 h Crab observation, after ALPHA cut						
ALPHA < (°)	30	15	9	9	6	5
N_γ/10 h	5779	3842	1785	542	1138	793
N_h/10 h	61.3×10^4	14.7×10^4	11383	700	659	94

Table 5: Study of the Crab signal in SIZE bins. Statistics corresponding to figures 12 to 14.

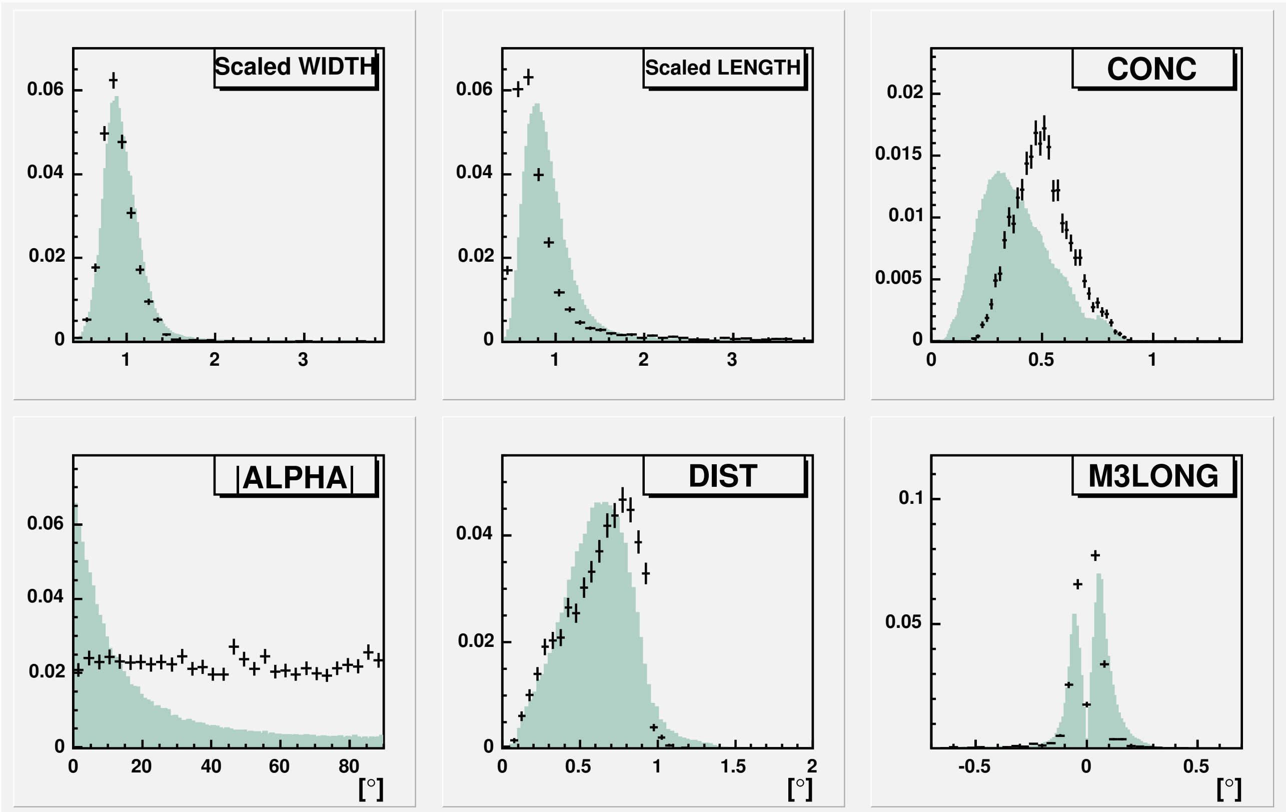

Figure 15: *Image parameter distributions for gammas (filled histograms) and hadrons (crosses), before γ/hadron separation, for the SIZE range 0 to 500 photons. M3LONG has a sign referred to the nominal source position (see text).*

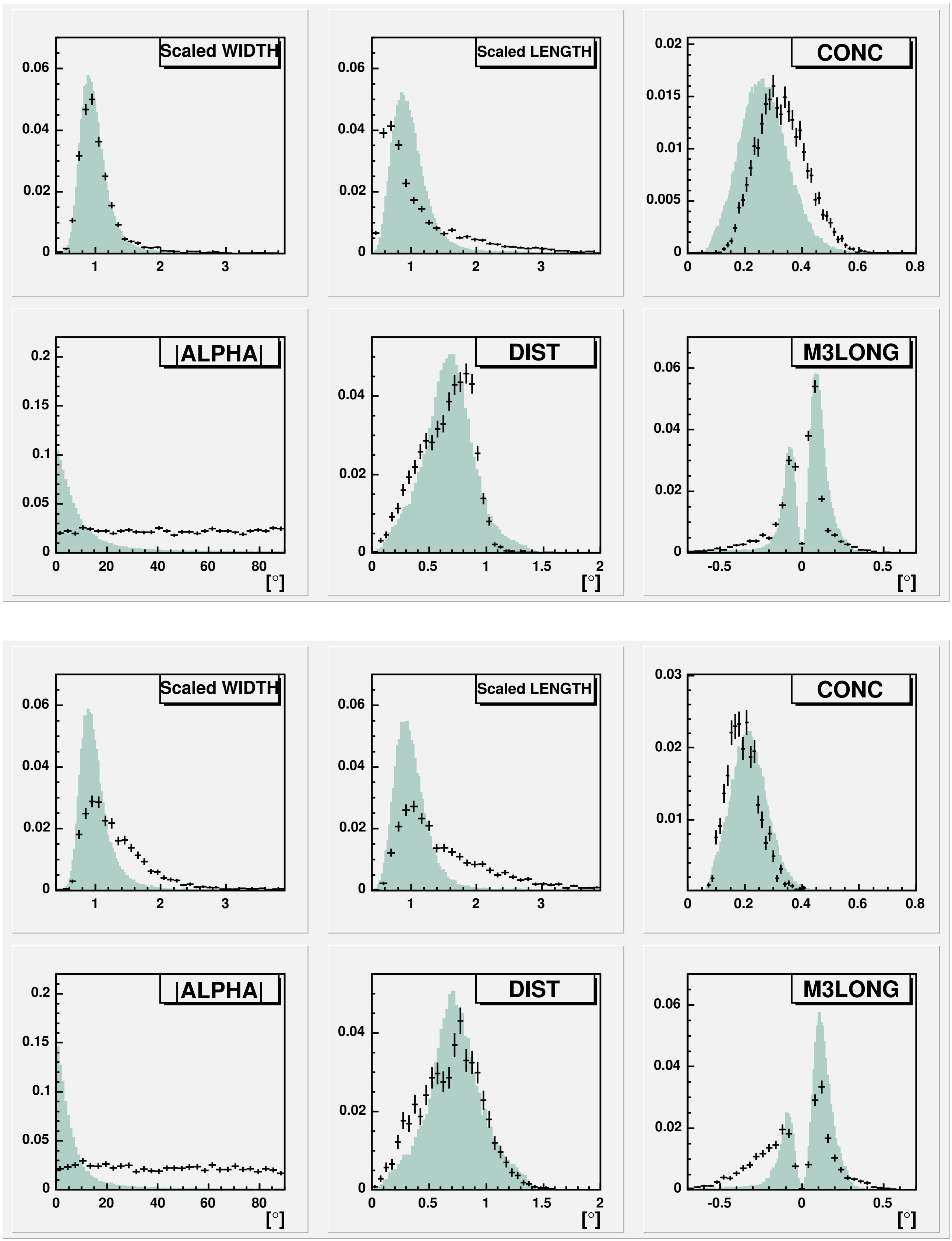

Figure 16: *Image parameter distributions for gammas (filled histograms) and hadrons (crosses), before γ/hadron separation, for the SIZE ranges 500 - 1000 (top) and 1000 - 2000 photons (bottom). M3LONG has a sign referred to the nominal source position (see text).*

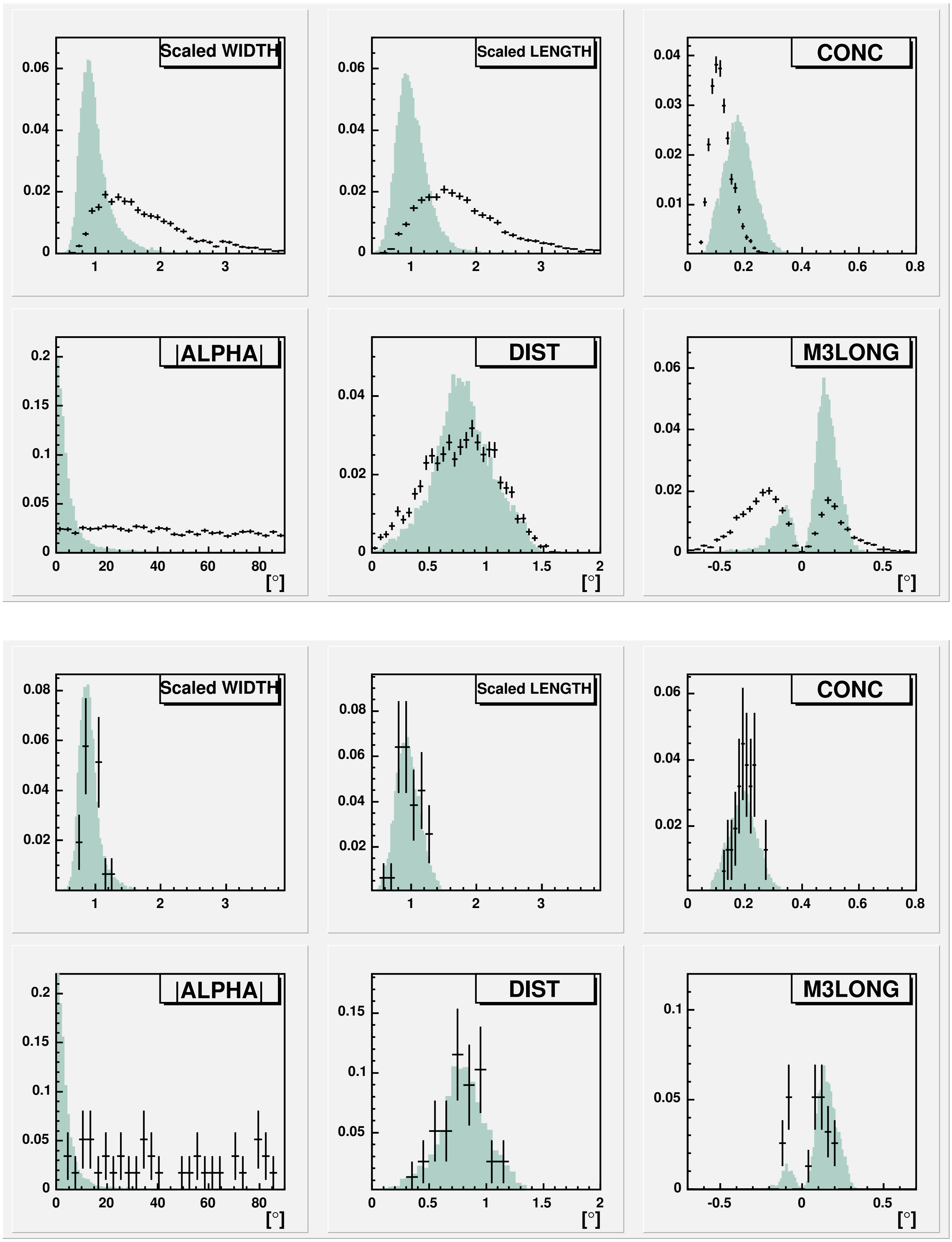

Figure 17: *Image parameter distributions for gammas (filled histograms) and hadrons (crosses), for the SIZE range 2000 - 4000 photons. Top: before γ/hadron separation. M3LONG has a sign referred to the nominal source position (see text). Bottom: after γ/hadron separation (ALPHA not used)*

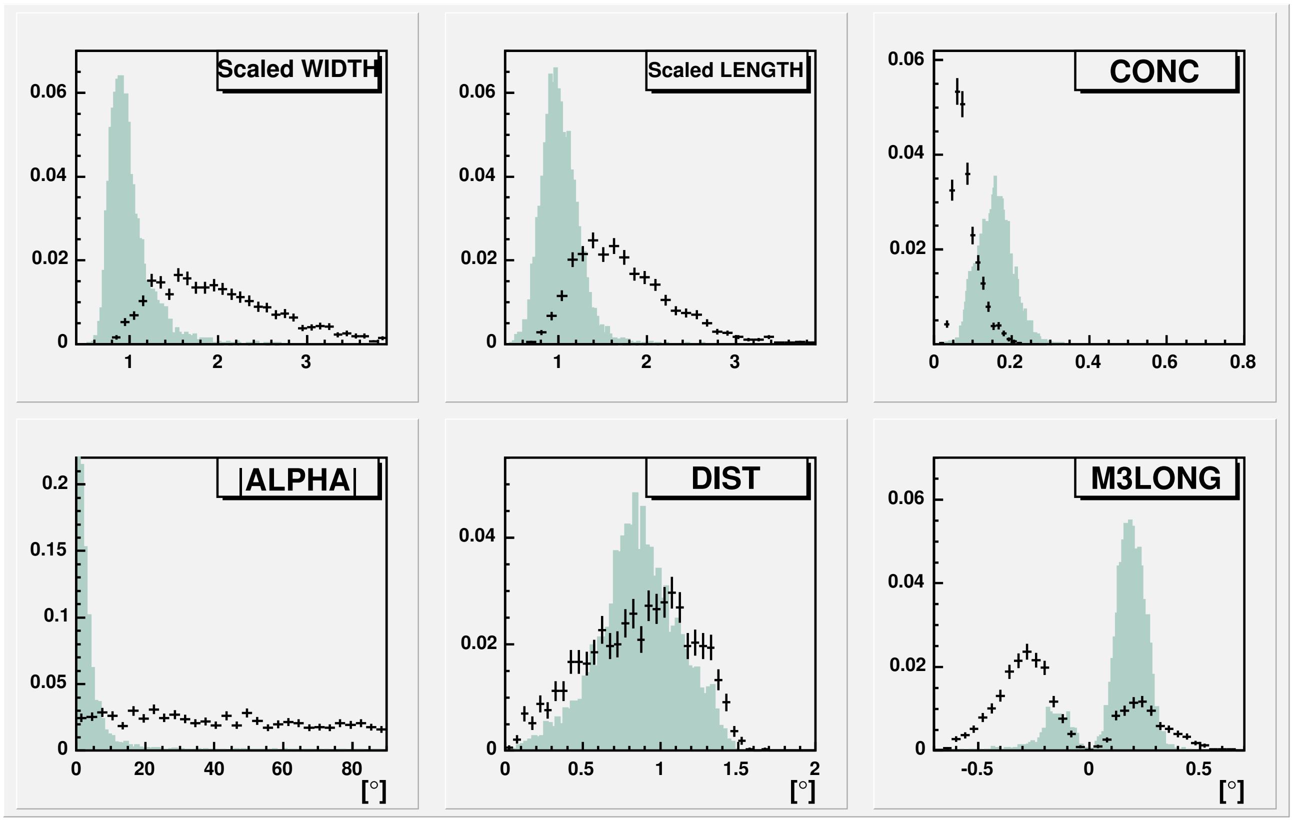

Figure 18: *Image parameter distributions for gammas (filled histograms) and hadrons (crosses), before γ/hadron separation, for the SIZE range 4000 - 8000 photons. M3LONG has a sign referred to the nominal source position (see text).*

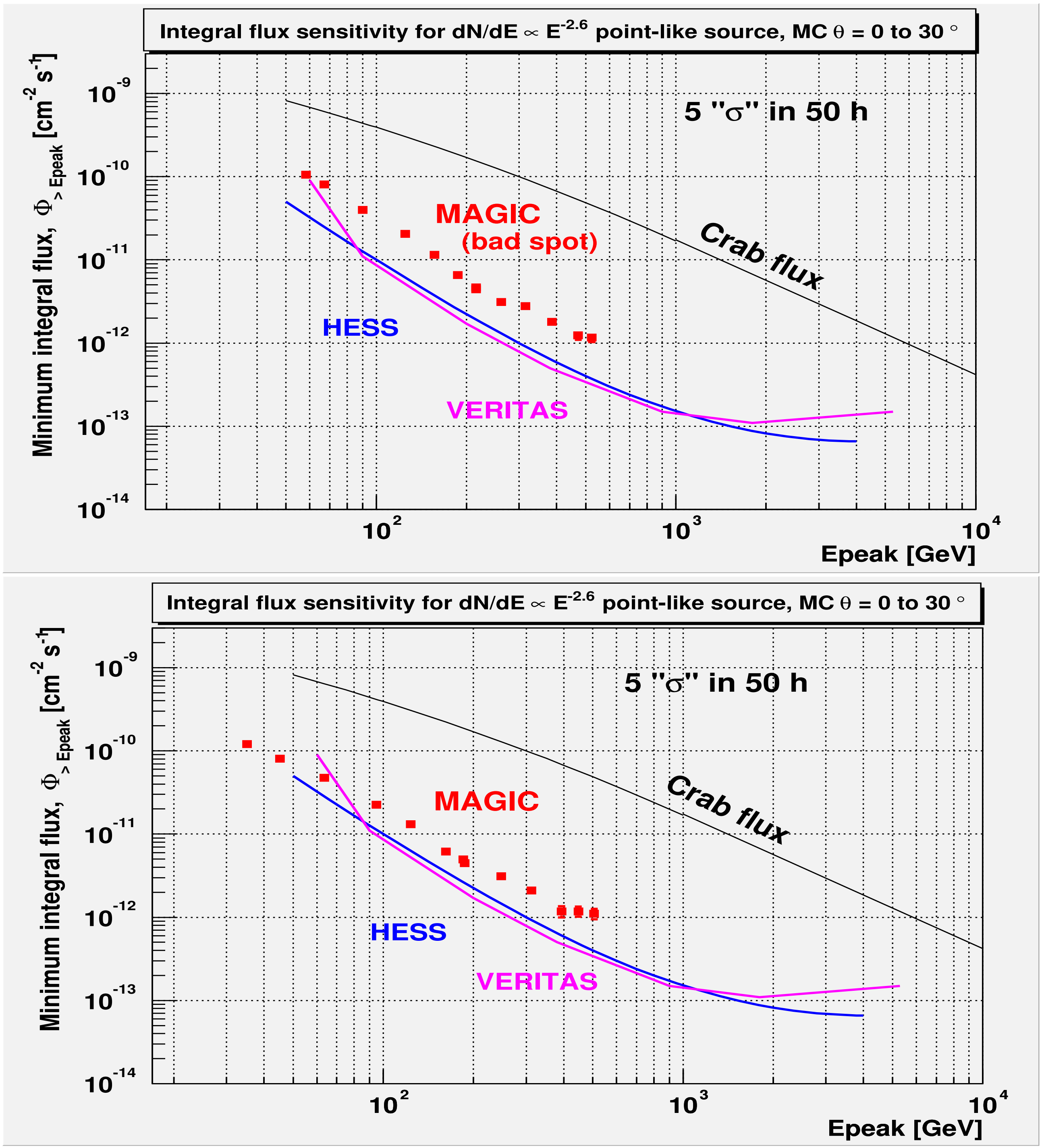

Figure 19: *Effect of a bad mirror performance on the MAGIC sensitivity. The plot above has been obtained with a mirror spot of about 0.1° (sigma of projected spot on x and y), thought to correspond to most of the data taken before the chess-boarding of the mirror panels in August. Below the sensitivity curve obtained assuming the current optical quality (the same as in the rest of this note). The MC simulation used in this two graphs is not exactly the same as described in §3, and this is why the lower plot has been included for comparison. Compared to the description in pg. 6, the camera simulation used for these plots has higher light collection efficiency (a 20% larger) and no FADC clock noise. These two features have little effect on sensitivity, the most visible being a somewhat lower energy threshold.*

References

[1] http://magic.pd.infn.it/mc_data/mc_index.html

[2] F. A. Aharonian et al. Astrophysical Journal 614, 897 (2004)

[3] AMS Collaboration, Physics Letters B 484 (2000)

[4] AMS Collaboration, Physics Letters B 490 (2000)

[5] AMS Collaboration, Physics Letters B 494 (2000)

[6] C. Baixeras et al, atro-ph/0403180 (2004)

[7] J. A. Barrio et al., The MAGIC telescope, Technical Design Report, MPI report, MPI-PHE/98-5 (1998)

[8] C. Bigongiari, A. Moralejo, V. Scalzotto, MAGIC-TDAS 03-01 (2003)

[9] O. Blanch, A. Moralejo, MAGIC-TDAS 04-07 How to use the camera simulation program 0.7 (2004)

[10] R. K. Bock et al, NIM A 516 (2003)

[11] M. Doro, Tesi di Laurea (2004) (in English)
http://www.magic.ifae.es/~mdoro/

[12] D. Heck et al, Report FZKA 6019 (1998)
http://www-ik.fzk.de/~heck/corsika/physics_description/corsika_phys.html

[13] T. Hengstebeck, User guide for the Mars Random Forest implementation (2003)
http://magic.physik.hu-berlin.de/protected/ranforest

[14] W. Hofmann, The HESS project, “The Universe viewed in gamma rays”, Kashiwa (2002). Slides available at
http://www.mpi-hd.mpg.de/hfm/HESS/public/publications/pub_talks.html

[15] K. Mase, muon ring studies (2004)
http://magic.mppmu.mpg.de/muc-group/analysis/muons/muon.html

[16] K. Mase, analysis of September 2004 Crab Nebula data (2004)
http://magic.mppmu.mpg.de/muc-group/analysis/crab/CrabSeptRF/CrabSeptRF.html

[17] F. Lucarelli et al. Astroparticle Physics 19, 339 (2003)

[18] R. Mirzoyan et al, New Astronomy Reviews 42, 547 (1998)

[19] A. Moralejo, G. Rossato, V. Scalzotto, C. Bigongiari, MAGIC-TDAS 04-05 (2004)

[20] A. Moralejo, presentation at the general MAGIC meeting in La Palma (2003)

http://wwwmagic.mppmu.mpg.de/meetings/minutes/cm-1003/Software/
Under: *4-Data Reconstruction* ⟶ *13-sensi2003oct.pdf*

[21] A. Moralejo, MAGIC-TDAS 02-11 (2002)

[22] D. Sobczyńska, MAGIC-TDAS 02-10 (2002)

[23] T. C. Weekes et al. Astroparticle Physics 17, 221 (2002)

[24] B. Wiebel-Sooth et al, Astronomy and Astrophysics 330 (1998)

[25] W. Wittek, MAGIC-TDAS 01-05 (2001)